



Article

# Bending, Free Vibration, and Buckling Analysis of Functionally Graded Porous Micro-Plates Using a General Third-Order Plate Theory

Semsi Coskun <sup>1</sup>, Jinseok Kim <sup>2,\*</sup> and Houssam Toutanji <sup>1</sup>

<sup>1</sup> Department of Civil and Construction Engineering, Western Michigan University, Kalamazoo, MI 49008, USA; semsi.coskun@wmich.edu (S.C.); houssam.toutanji@wmich.edu (H.T.)

<sup>2</sup> Department of Mechanical and Aerospace Engineering, Western Michigan University, Kalamazoo, MI 49008, USA

\* Correspondence: jinseok.kim@wmich.edu; Tel.: +1-269-276-3440

Received: 15 January 2019; Accepted: 28 January 2019; Published: 1 February 2019



**Abstract:** Static bending, free vibration and buckling of functionally graded porous micro-plates are investigated using a general third order plate theory. In addition, analytical solutions are obtained using the Navier method. The effect of the material length scale factor and the variation of material property through the thickness direction of plates are considered as well as porosity effects. Three different porosity distributions are considered and the effects of porosity variations are examined in the framework of a general third order plate theory. Numerical results show that the effect of each distribution of porosity is distinguished due to coupling between the heterogeneity of the material properties and the variation of porosity.

**Keywords:** third-order shear deformation plate theory; functionally graded porous materials; modified couple stress theory; analytical solution

## 1. Introduction

Micro electromechanical systems (MEMS) and Nano electromechanical systems (NEMS) are intelligent miniaturized systems used in many electronic devices, information/communication systems, chemical applications, and biomechanics [1]. The most of the structures used in MEMS and NEMS are in the form of beams and plates which can undergo deformation with the action of various loading cases. Studies show that the deformation of these small structures exhibits size dependency [2–9], which cannot be captured using the classical elasticity theory [3]. Hence, researchers have been studying new formulations which take into account the size dependency. The couple stress theory [10–12], Erigen's nonlocal elasticity theory [13] and the strain gradient plasticity theories [2,14] are the examples of the continuum theories which can be used to capture the size dependent behavior of small scaled structures.

Functionally graded materials (FGMs) are composite materials that have a smooth variation of the material properties within a body. These novel materials have several advantages including reduced in-plane and transverse stresses, low residual stresses [15,16], high thermal resistance, low thermal conductivity, and high fracture toughness [17,18]. Also, contrary to classical laminated composites, FGMs do not exhibit interlaminar stresses because of the smooth variation of material composition [18]. In addition, the variation of the material properties can be optimized and adjusted for the requirements. Hence, many researchers have been taken advantages of these novel materials using them in various engineering fields.

Reddy [19] developed a microstructure-dependent nonlinear Euler-Bernoulli and Timoshenko beam models based on the modified couple stress theory [12]. Analytical solutions to bending, natural

vibration and the buckling of homogeneous and functionally graded beams were provided. The newly developed model could capture the stiffening effect (size dependency) of small structures in bending and free vibration problems. It was shown that the difference in the deflections and frequencies decrease as the beam thickness increases.

Another study which also accounts for the size effect on functionally graded micro-beams was presented by Ke and Wang [7]. They investigated the influence of length scale parameter, power-law index, and length-to-thickness ratio on the dynamic stability of functionally graded micro-beams with several boundary conditions. Their parametric study showed that the micro-beams whose thicknesses were similar to their material length scale parameter experience a significant size effect in their free vibration, static buckling and dynamic characteristics. Simsek and Reddy analyzed functionally graded micro-beams with a higher order beam theory and modified couple stress theory [18]. Their study also emphasized that size effects became prominent as the thickness of the micro-beam and the material length-scale parameter are similar in magnitude. Li et al. [20] conducted a free vibration analysis of functionally graded beams with size-dependent Timoshenko beam model based on the strain gradient theory. Their study indicated that variation of material properties through the beam thickness had an important effect on the natural frequencies which could be used to control the natural frequencies. Their results also showed that the natural frequencies were in an increasing trend with increasing material length scale parameter.

In addition to FGM beams, mechanical responses of FGM plates have been investigated in the literature. Javaheri and Eslami [21] analyzed the buckling responses of functionally graded simply supported rectangular plate subjected to in-plane loading using the classical plate theory. Their result showed that the functionally graded plates resulted in smaller critical buckling loads than those of homogeneous plates. Hence, they noted that although functionally graded plates had numerous superior properties like heat resistance, their resistance should be checked against buckling failure. Nonlinear bending and the post-buckling behavior of functionally graded circular plates under mechanical and thermal loads were studied by Ma and Wang [22] based on von Kármán nonlinearity. Their study showed higher performance of functionally graded plates to resist thermal load or combination of thermal and mechanical load cases compared to fully metallic plate. They obtained lower temperature and deflection values than in pure metallic plates. Also, the effect of power-law index were discussed. Another study that investigated the thermal buckling of FGM plate was presented by Lanhe [23]. In this study, the equilibrium and stability equations of a simply supported moderately thick rectangular FGM plate were derived based on the first order shear deformation theory. The closed form solutions for the critical buckling temperature were obtained, and effects of plate aspect ratio, the relative thickness, the gradient index and the transverse shear on the buckling temperature were investigated. The results of the thick plates and plates with high aspect ratio showed that the critical buckling temperature was noticeably affected by the transverse shear deformation. In 2012, Reddy and Kim established a general third-order plate theory (GTPT) that accounted for the geometric nonlinearity, functionally graded material property, and microstructure-based size effects [24]. In GTPT, the material property variation was introduced in the plate constitutive relation. Also, the size effect was included by adopting Yang's modified couple stress theory [12]. Later, Kim and Reddy presented the Navier solutions of the bending, free vibration and buckling problems of functionally graded plates using GTPT [25]. Similarly, Thai and Choi developed size-dependent functionally graded Kirchhoff and Mindlin plate models based on Yang's modified couple stress theory [12]. The analytical solutions for deflection, buckling and vibration problems were presented in their study. Ansari et al. [26] investigated the size dependent vibration behavior of FG rectangular Mindlin micro-plates taking into account the geometric nonlinearity. Another size-dependent plate theory was developed by Zhang et al. [27]. Their model was based on the strain gradient theory and a newly developed refined shear deformation theory. The analyses of static bending, free vibration and buckling for functionally graded micro-plates resting on elastic foundation were conducted. Similar to the previous studies, the material length scale factor resulted in an increase in the stiffness of the

functionally graded micro-plate. Also, the size dependent model was more influenced by the effect of the transverse shear deformation compared to the classical models which did not include material length scale parameter in the formulation.

It is shown that FGMs can be further improved in terms of weight reduction and energy absorption by introducing the porosity while maintaining a significant amount of strength [28,29]. There are various studies in the literature which show that the functionally graded porous materials (FGPMs) have promising results for several engineering applications such as enhanced filtration [30], automotive industry [31], and medical implants [32,33]. Hence, numerous researchers investigated the mechanical responses of the FGPMs, as the new class of composite materials.

Elastic buckling and static bending analysis of functionally graded porous beams were performed by Chen et al. [9] based on Timoshenko beam theory. Their study showed that as the porosity and the slenderness of the beam increased, the critical buckling load decreased and the maximum deflections obtained from bending analysis increased. Moreover, the buckling and the bending analysis were significantly affected by the porosity distribution. Later, Chen et al. [34] conducted free and forced vibration analysis of functionally graded beams with symmetric and asymmetric porosity distributions. They concluded that the symmetric porosity distribution resulted better beam stiffness; hence, higher fundamental frequency and lower dynamic deflection compared to the asymmetric one. Shafiei and Kazemi [35] presented the buckling analysis of two-dimensional functionally graded porous tapered Euler-Bernoulli nano- and micro-beams. The size effect was included using the modified couple stress theory. A modified series solution for free vibration analyses of moderately thick functionally graded porous deep curved and straight beams with general boundary conditions were proposed by Zhao et al. [36]. Their results showed that the highest frequencies were obtained by the FGP beams with symmetric porosity distribution, but the lowest frequencies were resulted by the FGP beams with uniform porosity distribution. In addition to geometric and material parameters, the boundary conditions strongly influenced the vibration characteristics of FGM beams. A finite element analysis was performed on free and forced vibration of functionally graded porous beam and frame structures by Wu et al. [37]. Their approach was tested with several numerical examples and the results were compared with both analytical and experimental results.

Shahverdi and Barati [38] developed a general nonlocal strain gradient elasticity model, and the vibration analysis of functionally graded porous nano-plates were carried out. To obtain more accurate predictions, two scale parameters were included in their proposed model. The derived governing equations of nano-plate were solved for natural frequencies by using the Galerkin method. It was demonstrated that the porosity had an important effect on mechanical behavior. They concluded that both nonlocal and strain gradient parameters were needed to capture both stiffness-softening and stiffness-hardening effects in the modeling of nano-plates. Wang et al. [39] investigated the vibrations of the longitudinally traveling functionally graded plates with both evenly and unevenly distributed porosity. The effects of porosity, damping and constituent fraction on the dynamic response of FGPM plates were examined. An analytical approach for natural frequencies of the functionally graded porous plates were established by Rezaei et al. [40]. Their model was based on the four variable refined plate theory of Thai and Choi [41], which is a modified first order shear theory. The effect of porosity, power-law index, thickness-side ratio, aspect ratio, porosity distribution and the boundary conditions of the rectangular plate were examined. Akbas [42] presented a vibration and the static bending analysis of a simply supported functionally graded porous rectangular plate within the framework of first order shear deformation theory. Wang and Zu [43] investigated the large-amplitude vibration of sigmoid functionally graded thin plates with porosities. The geometric nonlinearities were included by adopting von Kármán nonlinear plate theory. Their results indicated that even and uneven distribution types of porosity had different effects on the resonance domain of sigmoid functionally graded plates. Besides, the effect of the constituent volume distribution was clearly shown. The nonlinear thermomechanical buckling and post buckling response of porous functionally graded plates were studied by Cong et al. [44]. Their formulations were based on Reddy's higher-order

shear deformation theory. Their results demonstrated that better performance of the plate with evenly distributed porosity in terms of buckling and post-buckling analysis. Also, Pasternak shear layer stiffness gave a significant effect over Winkler elastic modulus on the porous functionally graded plate nonlinear stability. The transient response of porous functionally graded nano-plates under various pulse loads were investigated by Mirjavadi et al. [45] in the framework of nonlocal strain gradient theory. The effects of nonlocal coefficient, strain gradient parameter, porosity, type of impulse and the loading time on the transient response were discussed. Zhao et al. [46] established a novel three-dimensional exact solution for vibration analysis of thick FGPM plates with three different porosity distributions. Then, Zhao et al. [47] conducted an extensive study on the dynamic analysis of FGP circular, annular and sector plates with general elastic restraints. Thang et al. [48] performed elastic buckling and free vibration analyses of porous-cellular plates with various porosity distributions. Bending, free vibration and buckling analyses of FGP micro-plates were conducted by Kim et al. [49]. In their study, both the classical and first order shear theory were used with modified couple stress theory. Because they only studied the classical and first order shear deformation theory, their models cannot properly account for the parabolic transverse shear deformation.

Contrary to majority of the previous studies on functionally graded porous plates, this work presents the analysis of FGP plates with a higher order shear deformation theory that provides more accurate transverse shear stresses. Moreover, by using the general third-order plate theory [24], this study accounts for the thickness deformation of plates. In addition, the effect of porosity distribution, the size-dependency and the smooth change in the material property through the thickness direction of the plate are considered. The effect of several types of porosity distributions to the FGM micro-plates is investigated more precisely, and the numerical results of the bending, free vibration and buckling analysis are presented in this work.

## 2. General Third-Order Plate Theory

The classical plate theory (CPT) is based on the assumption that straight lines perpendicular to the mid-plane of the plate in the undeformed configuration remains straight, inextensible and perpendicular to the mid-plane of the plate after the deformation. The first order shear deformation plate theory + (FSDT) releases the normality condition. However, it requires a shear correction factor because the resulted transverse shear strains are nonzero but independent of the thickness coordinate,  $z$ . In addition to the normality condition, the general third order shear deformation plate theory (GTPT) [50] further releases the straight and the inextensibility conditions by expanding the displacement fields as cubic functions of  $z$ . Hence, the necessity of the shear correction factor is avoided by achieving the desired quadratic variation of the transverse shear strains and stresses through the plate thickness.

### 2.1. Displacements and Strains

In the GTPT, displacement field is extended up to third power of thickness coordinate for in plane displacements and second power of thickness coordinate for out of plane displacement [24]. The assumed displacement field is

$$\begin{aligned}
 u_1(x, y, z, t) &= u(x, y, t) + z\theta_x(x, y, t) + z^2\phi_x(x, y, t) + z^3\psi_x(x, y, t) \\
 u_2(x, y, z, t) &= v(x, y, t) + z\theta_y(x, y, t) + z^2\phi_y(x, y, t) + z^3\psi_y(x, y, t) \\
 u_3(x, y, z, t) &= w(x, y, t) + z\theta_z(x, y, t) + z^2\phi_z(x, y, t)
 \end{aligned}
 \tag{1}$$

where  $u, v, w, \theta_x, \theta_y, \theta_z, \phi_x, \phi_y, \phi_z, \psi_x$ , and  $\psi_y$  are unknown generalized displacements. The linearized strains of the GTPT are (see Reddy and Kim [24]):

$$\begin{pmatrix} \varepsilon_{xx} \\ \varepsilon_{yy} \\ \varepsilon_{zz} \\ \gamma_{xy} \\ \gamma_{xz} \\ \gamma_{yz} \end{pmatrix} = \begin{pmatrix} \varepsilon_{xx}^{(0)} \\ \varepsilon_{yy}^{(0)} \\ \varepsilon_{zz}^{(0)} \\ \gamma_{xy}^{(0)} \\ \gamma_{xz}^{(0)} \\ \gamma_{yz}^{(0)} \end{pmatrix} + z \begin{pmatrix} \varepsilon_{xx}^{(1)} \\ \varepsilon_{yy}^{(1)} \\ \varepsilon_{zz}^{(1)} \\ \gamma_{xy}^{(1)} \\ \gamma_{xz}^{(1)} \\ \gamma_{yz}^{(1)} \end{pmatrix} + z^2 \begin{pmatrix} \varepsilon_{xx}^{(2)} \\ \varepsilon_{yy}^{(2)} \\ \varepsilon_{zz}^{(2)} \\ \gamma_{xy}^{(2)} \\ \gamma_{xz}^{(2)} \\ \gamma_{yz}^{(2)} \end{pmatrix} + z^3 \begin{pmatrix} \varepsilon_{xx}^{(3)} \\ \varepsilon_{yy}^{(3)} \\ \varepsilon_{zz}^{(3)} \\ \gamma_{xy}^{(3)} \\ \gamma_{xz}^{(3)} \\ \gamma_{yz}^{(3)} \end{pmatrix} \tag{2}$$

where the nonzero strains are given as

$$\begin{aligned} \varepsilon_{xx}^{(0)} &= \frac{\partial u}{\partial x}, & \varepsilon_{xx}^{(1)} &= \frac{\partial \theta_x}{\partial x}, & \varepsilon_{xx}^{(2)} &= \frac{\partial \phi_x}{\partial x}, & \varepsilon_{xx}^{(3)} &= \frac{\partial \psi_x}{\partial x}, \\ \varepsilon_{yy}^{(0)} &= \frac{\partial v}{\partial y}, & \varepsilon_{yy}^{(1)} &= \frac{\partial \theta_y}{\partial y}, & \varepsilon_{yy}^{(2)} &= \frac{\partial \phi_y}{\partial y}, & \varepsilon_{yy}^{(3)} &= \frac{\partial \psi_y}{\partial y}, \\ \varepsilon_{zz}^{(0)} &= \theta_z, & \varepsilon_{zz}^{(1)} &= 2\phi_z, & \gamma_{xy}^{(0)} &= \frac{\partial u}{\partial y} + \frac{\partial v}{\partial x}, & \gamma_{xy}^{(1)} &= \frac{\partial \theta_x}{\partial y} + \frac{\partial \theta_y}{\partial x}, \\ \gamma_{xy}^{(2)} &= \frac{\partial \phi_x}{\partial y} + \frac{\partial \phi_y}{\partial x}, & \gamma_{xy}^{(3)} &= \frac{\partial \psi_x}{\partial y} + \frac{\partial \psi_y}{\partial x}, & \gamma_{xz}^{(0)} &= \theta_x + \frac{\partial w}{\partial x}, & \gamma_{xz}^{(1)} &= 2\phi_x + \frac{\partial \theta_z}{\partial x}, \\ \gamma_{xz}^{(2)} &= 3\psi_x + \frac{\partial \phi_z}{\partial x}, & \gamma_{yz}^{(0)} &= \theta_y + \frac{\partial w}{\partial y}, & \gamma_{yz}^{(1)} &= 2\phi_y + \frac{\partial \theta_z}{\partial y}, & \gamma_{yz}^{(2)} &= 3\psi_y + \frac{\partial \phi_z}{\partial y}. \end{aligned} \tag{3}$$

### 2.2. Modified Couple Stress Model

In the classical couple stress theory [10,11], a couple that leads to the particle to rotate as well as a force to translate are considered as the applied loads on material particle. Equilibrium equations of the forces and the moments of the forces are satisfied as those in the case of classical elasticity. The strain and curvature tensors are the deformation tensors which are conjugated with the stress and the couple stress tensors, respectively. In addition to the Lamé constants, two independent length scale parameters exist associated with the symmetric and the antisymmetric parts of the curvature tensor in the constitutive relation. However, it requires extensive experiments to determine these two length scale parameters. In 2002, Yang et al. proposed the modified couple stress theory [12] and showed that only one single length scale parameter is adequate to include size effect for linear isotropic elastic materials. They achieved this result by enforcing higher order equilibrium equations which restrict the couple stress tensor to be symmetric [12]. Hence, only the symmetric part of the curvature tensor contributes to the strain energy density and the only one length scale parameter associated with the symmetric part of the curvature tensor is required [12,24].

The expression for the virtual strain energy  $\delta U$  using the modified couple stress theory is [24]

$$\delta U = \int_V (\delta \varepsilon : \sigma + \delta \chi : \mathbf{m}) dv = \int_V (\sigma_{ij} \delta \varepsilon_{ij} + m_{ij} \delta \chi_{ij}) dv \tag{4}$$

where summation on repeated indices is implied; here  $\sigma_{ij}$  and  $m_{ij}$  denote the Cartesian components of symmetric stress tensor and the deviatoric couple stress tensor, respectively. For the linear elastic solid material, they can be expressed as the following form

$$\begin{aligned} \sigma_{ij} &= \lambda \varepsilon_{ii} \delta_{ij} + 2\mu \varepsilon_{ij}, \\ m_{ij} &= 2\mu l^2 \chi_{ij} \end{aligned} \tag{5}$$

where  $\lambda$  and  $\mu$  are the Lamé constants,  $l$  is the material length scale parameter that can represents the size dependency in small scale structures, and  $\delta_{ij}$  is the Kronecker's delta. The components of

the linear strain tensor, i.e.,  $\varepsilon_{ij}$  are given in Equations (2) and (3). The components of the symmetric curvature tensor  $\chi_{ij}$  are

$$\chi = \frac{1}{2} [\nabla \omega + (\nabla \omega)^T], \quad \omega = \frac{1}{2} \nabla \times \mathbf{u} \tag{6}$$

or

$$\chi_{ij} = \frac{1}{2} \left( \frac{\partial \omega_i}{\partial x_j} + \frac{\partial \omega_j}{\partial x_i} \right), \quad i, j = 1, 2, 3 \tag{7}$$

and  $\omega_i$  ( $i = 1, 2, 3$ ) are the components of the rotation vector can be expressed as

$$\omega_x = \omega_1 = \frac{1}{2} \left( \frac{\partial u_3}{\partial x_2} - \frac{\partial u_2}{\partial x_3} \right), \quad \omega_y = \omega_2 = \frac{1}{2} \left( \frac{\partial u_1}{\partial x_3} - \frac{\partial u_3}{\partial x_1} \right), \quad \omega_z = \omega_3 = \frac{1}{2} \left( \frac{\partial u_2}{\partial x_1} - \frac{\partial u_1}{\partial x_2} \right). \tag{8}$$

Substituting the rotation vector  $\omega_i$  ( $i = 1, 2, 3$ ) into the above vector equation, the components of the symmetric curvature tensor result

$$\begin{aligned} \chi_{xx} = \chi_{11} &= \frac{1}{2} \left( \frac{\partial^2 u_3}{\partial x_1 \partial x_2} - \frac{\partial^2 u_2}{\partial x_1 \partial x_3} \right), \\ \chi_{yy} = \chi_{22} &= \frac{1}{2} \left( \frac{\partial^2 u_1}{\partial x_2 \partial x_3} - \frac{\partial^2 u_3}{\partial x_1 \partial x_2} \right), \\ \chi_{zz} = \chi_{33} &= \frac{1}{2} \left( \frac{\partial^2 u_2}{\partial x_1 \partial x_3} - \frac{\partial^2 u_1}{\partial x_2 \partial x_3} \right), \\ \chi_{xy} = 2\chi_{12} &= \frac{1}{2} \left( \frac{\partial^2 u_3}{\partial x_2^2} - \frac{\partial^2 u_2}{\partial x_2 \partial x_3} + \frac{\partial^2 u_1}{\partial x_1 \partial x_3} - \frac{\partial^2 u_3}{\partial x_1^2} \right), \\ \chi_{xz} = 2\chi_{13} &= \frac{1}{2} \left( \frac{\partial^2 u_3}{\partial x_2 \partial x_3} - \frac{\partial^2 u_2}{\partial x_3^2} + \frac{\partial^2 u_2}{\partial x_1^2} - \frac{\partial^2 u_1}{\partial x_1 \partial x_2} \right), \\ \chi_{yz} = 2\chi_{23} &= \frac{1}{2} \left( \frac{\partial^2 u_1}{\partial x_3^2} - \frac{\partial^2 u_3}{\partial x_1 \partial x_3} + \frac{\partial^2 u_2}{\partial x_1 \partial x_2} - \frac{\partial^2 u_1}{\partial x_2^2} \right). \end{aligned}$$

which can be written as

$$\begin{Bmatrix} \chi_{xx} \\ \chi_{yy} \\ \chi_{zz} \\ \chi_{xy} \\ \chi_{xz} \\ \chi_{yz} \end{Bmatrix} = \begin{Bmatrix} \chi_{xx}^{(0)} \\ \chi_{yy}^{(0)} \\ \chi_{zz}^{(0)} \\ \chi_{xy}^{(0)} \\ \chi_{xz}^{(0)} \\ \chi_{yz}^{(0)} \end{Bmatrix} + z \begin{Bmatrix} \chi_{xx}^{(1)} \\ \chi_{yy}^{(1)} \\ \chi_{zz}^{(1)} \\ \chi_{xy}^{(1)} \\ \chi_{xz}^{(1)} \\ \chi_{yz}^{(1)} \end{Bmatrix} + z^2 \begin{Bmatrix} \chi_{xx}^{(2)} \\ \chi_{yy}^{(2)} \\ \chi_{zz}^{(2)} \\ \chi_{xy}^{(2)} \\ \chi_{xz}^{(2)} \\ \chi_{yz}^{(2)} \end{Bmatrix} + z^3 \begin{Bmatrix} \chi_{xx}^{(3)} \\ \chi_{yy}^{(3)} \\ \chi_{zz}^{(3)} \\ \chi_{xy}^{(3)} \\ \chi_{xz}^{(3)} \\ \chi_{yz}^{(3)} \end{Bmatrix} \tag{9}$$

where the nonzero components in terms of generalized displacements are obtained as

$$\begin{aligned} \chi_{xx}^{(0)} &= \frac{1}{2} \left[ \frac{\partial}{\partial x} \left( \frac{\partial w}{\partial y} - \theta_y \right) \right], \quad \chi_{xx}^{(1)} = \frac{1}{2} \left[ \frac{\partial}{\partial x} \left( \frac{\partial \theta_z}{\partial y} - 2\phi_y \right) \right], \quad \chi_{xx}^{(2)} = \frac{1}{2} \left[ \frac{\partial}{\partial x} \left( \frac{\partial \phi_z}{\partial y} - 3\psi_y \right) \right], \\ \chi_{yy}^{(0)} &= \frac{1}{2} \left[ \frac{\partial}{\partial y} \left( \theta_x - \frac{\partial w}{\partial x} \right) \right], \quad \chi_{yy}^{(1)} = \frac{1}{2} \left[ \frac{\partial}{\partial y} \left( 2\phi_x - \frac{\partial \theta_z}{\partial x} \right) \right], \quad \chi_{yy}^{(2)} = \frac{1}{2} \left[ \frac{\partial}{\partial x} \left( 3\psi_x - \frac{\partial \phi_z}{\partial x} \right) \right], \\ \chi_{zz}^{(0)} &= \frac{1}{2} \left( \frac{\partial \theta_y}{\partial x} - \frac{\partial \theta_x}{\partial y} \right), \quad \chi_{zz}^{(1)} = \left( \frac{\partial \phi_y}{\partial x} - \frac{\partial \phi_x}{\partial y} \right), \quad \chi_{zz}^{(2)} = \frac{3}{2} \left( \frac{\partial \psi_y}{\partial x} - \frac{\partial \psi_x}{\partial y} \right), \\ \chi_{xy}^{(0)} &= \frac{1}{2} \left[ \frac{\partial}{\partial y} \left( \frac{\partial w}{\partial y} - \theta_y \right) + \frac{\partial}{\partial x} \left( \theta_x - \frac{\partial w}{\partial x} \right) \right], \quad \chi_{xy}^{(1)} = \frac{1}{2} \left[ \frac{\partial}{\partial y} \left( \frac{\partial \theta_z}{\partial y} - 2\phi_y \right) + \frac{\partial}{\partial x} \left( 2\phi_x - \frac{\partial \theta_z}{\partial x} \right) \right], \\ \chi_{xy}^{(2)} &= \frac{1}{2} \left[ \frac{\partial}{\partial y} \left( \frac{\partial \phi_z}{\partial y} - 3\psi_y \right) + \frac{\partial}{\partial x} \left( 3\psi_x - \frac{\partial \phi_z}{\partial x} \right) \right], \end{aligned}$$

$$\begin{aligned} \chi_{xz}^{(0)} &= \frac{1}{2} \left[ \frac{\partial}{\partial x} \left( \frac{\partial v}{\partial x} - \frac{\partial u}{\partial y} \right) + \frac{\partial \theta_z}{\partial y} - 2\phi_y \right], \quad \chi_{xz}^{(1)} = \frac{1}{2} \left[ \frac{\partial}{\partial x} \left( \frac{\partial \theta_y}{\partial x} - \frac{\partial \theta_x}{\partial y} \right) + 2 \left( \frac{\partial \phi_z}{\partial y} - 3\psi_y \right) \right], \\ \chi_{xz}^{(2)} &= \frac{1}{2} \left[ \frac{\partial}{\partial x} \left( \frac{\partial \phi_z}{\partial y} - 3\psi_y \right) + \frac{\partial}{\partial x} \left( 3\psi_x - \frac{\partial \phi_z}{\partial x} \right) \right], \quad \chi_{xz}^{(3)} = \frac{1}{2} \frac{\partial}{\partial x} \left( \frac{\partial \psi_y}{\partial x} - \frac{\partial \psi_x}{\partial y} \right), \\ \chi_{yz}^{(0)} &= \frac{1}{2} \left[ \frac{\partial}{\partial y} \left( \frac{\partial v}{\partial x} - \frac{\partial u}{\partial y} \right) + 2\phi_x - \frac{\partial \theta_z}{\partial x} \right], \quad \chi_{yz}^{(1)} = \frac{1}{2} \left[ \frac{\partial}{\partial y} \left( \frac{\partial \theta_y}{\partial x} - \frac{\partial \theta_x}{\partial y} \right) + 2 \left( 3\psi_x - \frac{\partial \phi_z}{\partial x} \right) \right], \\ \chi_{yz}^{(2)} &= \frac{1}{2} \left[ \frac{\partial}{\partial y} \left( \frac{\partial \phi_z}{\partial y} - 3\psi_y \right) + \frac{\partial}{\partial x} \left( 3\psi_x - \frac{\partial \phi_z}{\partial x} \right) \right], \quad \chi_{yz}^{(3)} = \frac{1}{2} \frac{\partial}{\partial y} \left( \frac{\partial \psi_y}{\partial x} - \frac{\partial \psi_x}{\partial y} \right). \end{aligned}$$

### 2.3. FGPM Plate Constitutive Equations

In this study, isotropic plates with variation of two constituents and distribution of porosity through thickness are assumed. The considered three different porosity distributions [49] are

$$\begin{aligned} \text{Type 1: } \Phi(z) &= \phi \cos \left[ \pi \left( \frac{z}{h} \right) \right] \\ \text{Type 2: } \Phi(z) &= \phi \cos \left[ \frac{\pi}{2} \left( \frac{z}{h} + \frac{1}{2} \right) \right] \\ \text{Type 3: } \Phi(z) &= \phi \cos \left[ \frac{\pi}{2} \left( \frac{z}{h} - \frac{1}{2} \right) \right] \end{aligned} \tag{10}$$

where  $\phi$  is the maximum porosity value achieved by the distribution. A typical material property of the functionally graded porous materials (FGPM) can be considered as in the following power-law relations [49],

$$P(z) = \left[ (P_t - P_b) \left( \frac{z}{h} + \frac{1}{2} \right)^n + P_b \right] (1 - \Phi(z)) \tag{11}$$

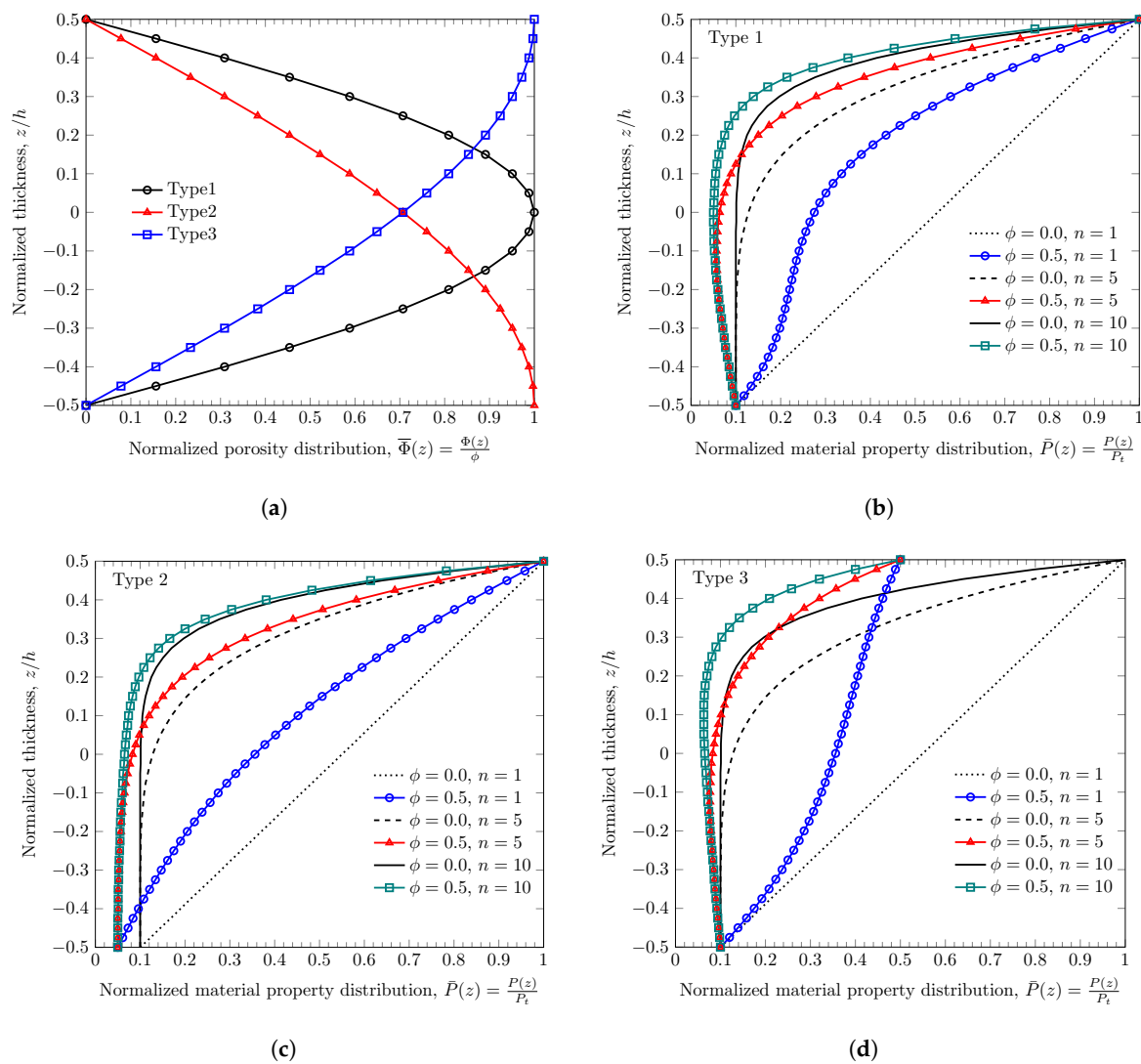
where  $P_t$  and  $P_b$  are the typical material properties at the top and the bottom surfaces, respectively and  $n$  is the power-law index.

Figure 1 shows the normalized porosity and the material property distributions through the plate thickness. For the illustration purpose, the material property at the top surface is assumed as ten times larger than the material property at the bottom surface of the plate and the porosity value of  $\phi = 0.5$  is taken. As can be seen in Figure 1a, all three types of porosity distribution result in the same volume of void through the material. However, the Type 1 distribution is symmetric about the mid-plane of the plate. Also, the middle section of the plate is more porous and the porosity of the material decreases through the top and the bottom surfaces in the case of Type 1 distribution. On the other hand, this symmetry is not valid for porosity distribution Type 2 and 3. In the case of Type 2, the porosity increases zero at the top surface to assigned  $\phi$  value at the bottom surface of the plate. Type 3 porosity distribution has the opposite variation to the Type 2.

Figure 1b–d demonstrate the effect of power-law index,  $n$  and porosity distribution types on the variation of material properties. As can be seen from Figure 1b–d, the distributions of the normalized material property with Type 1 and Type 2 show similar trend, but Type 3 exhibits quite different variation. This is because the material on top surface is assumed to be stiffer than the material on bottom surface.

Under isothermal conditions, the linear constitutive relation for an isotropic plate is given by

$$\begin{Bmatrix} \sigma_{xx} \\ \sigma_{yy} \\ \sigma_{zz} \\ \sigma_{xy} \\ \sigma_{xz} \\ \sigma_{yz} \end{Bmatrix} = \frac{E}{(1 + \nu)(1 - 2\nu)} \begin{bmatrix} 1 - \nu & \nu & \nu & 0 & 0 & 0 \\ \nu & 1 - \nu & \nu & 0 & 0 & 0 \\ \nu & \nu & 1 - \nu & 0 & 0 & 0 \\ 0 & 0 & 0 & \frac{1}{2}(1 - 2\nu) & 0 & 0 \\ 0 & 0 & 0 & 0 & \frac{1}{2}(1 - 2\nu) & 0 \\ 0 & 0 & 0 & 0 & 0 & \frac{1}{2}(1 - 2\nu) \end{bmatrix} \begin{Bmatrix} \epsilon_{xx} \\ \epsilon_{yy} \\ \epsilon_{zz} \\ \epsilon_{xy} \\ \epsilon_{xz} \\ \epsilon_{yz} \end{Bmatrix} \tag{12}$$



**Figure 1.** The normalized porosity distribution through the plate thickness (a) and normalized material property resulted from Type 1 distribution (b); Type 2 distribution (c); and Type 3 distribution (d).

In the present study, Young’s modulus,  $E$ , varies through thickness direction but Poisson’s ratio,  $\nu$ , is assumed to be a constant in the constitutive Equation (12). The generalized forces and couples can be expressed as then

$$\begin{Bmatrix} M_{xx}^{(i)} \\ M_{yy}^{(i)} \\ M_{zz}^{(i)} \end{Bmatrix} = \int_{-\frac{h}{2}}^{\frac{h}{2}} \begin{Bmatrix} \sigma_{xx} \\ \sigma_{yy} \\ \sigma_{zz} \end{Bmatrix} (z)^i dz = \sum_{k=i}^{3+i} \begin{bmatrix} A_{11}^{(k)} & A_{12}^{(k)} & A_{12}^{(k)} \\ A_{12}^{(k)} & A_{11}^{(k)} & A_{12}^{(k)} \\ A_{12}^{(k)} & A_{12}^{(k)} & A_{11}^{(k)} \end{bmatrix} \begin{Bmatrix} \varepsilon_{xx}^{(k-i)} \\ \varepsilon_{yy}^{(k-i)} \\ \varepsilon_{zz}^{(k-i)} \end{Bmatrix} \quad (13)$$

$$\begin{Bmatrix} M_{xy}^{(i)} \\ M_{xz}^{(i)} \\ M_{yz}^{(i)} \end{Bmatrix} = \int_{-\frac{h}{2}}^{\frac{h}{2}} \begin{Bmatrix} \sigma_{xy} \\ \sigma_{xz} \\ \sigma_{yz} \end{Bmatrix} (z)^i dz = \sum_{k=i}^{3+i} \begin{bmatrix} B_{11}^{(k)} & 0 & 0 \\ 0 & B_{11}^{(k)} & 0 \\ 0 & 0 & B_{11}^{(k)} \end{bmatrix} \begin{Bmatrix} \gamma_{xy}^{(k-i)} \\ \gamma_{xz}^{(k-i)} \\ \gamma_{yz}^{(k-i)} \end{Bmatrix} \quad (14)$$

$$\begin{Bmatrix} \mathcal{M}_{xx}^{(i)} \\ \mathcal{M}_{yy}^{(i)} \\ \mathcal{M}_{zz}^{(i)} \end{Bmatrix} = \int_{-\frac{h}{2}}^{\frac{h}{2}} \begin{Bmatrix} m_{xx} \\ m_{yy} \\ m_{zz} \end{Bmatrix} (z)^i dz = \sum_{k=i}^{2+i} \begin{bmatrix} \mathcal{B}_{11}^{(k)} & 0 & 0 \\ 0 & \mathcal{B}_{11}^{(k)} & 0 \\ 0 & 0 & \mathcal{B}_{11}^{(k)} \end{bmatrix} \begin{Bmatrix} \chi_{xx}^{(k-i)} \\ \chi_{yy}^{(k-i)} \\ \chi_{zz}^{(k-i)} \end{Bmatrix} \quad (15)$$

$$\begin{Bmatrix} \mathcal{M}_{xy}^{(i)} \\ \mathcal{M}_{xz}^{(i)} \\ \mathcal{M}_{yz}^{(i)} \end{Bmatrix} = \int_{-\frac{h}{2}}^{\frac{h}{2}} \begin{Bmatrix} m_{xy} \\ m_{xz} \\ m_{yz} \end{Bmatrix} (z)^i dz = \sum_{k=i}^{3+i} \begin{bmatrix} \mathcal{B}_{11}^{(k)} & 0 & 0 \\ 0 & \mathcal{B}_{11}^{(k)} & 0 \\ 0 & 0 & \mathcal{B}_{11}^{(k)} \end{bmatrix} \begin{Bmatrix} \chi_{xy}^{(k-i)} \\ \chi_{xz}^{(k-i)} \\ \chi_{yz}^{(k-i)} \end{Bmatrix} \tag{16}$$

where  $m_{ij}$  and  $\sigma_{ij}$  are expressed in Equation (5), and plate stiffness ( $A_{11}, A_{12}, B_{11}$ , and  $\mathcal{B}_{11}$ ) are

$$\begin{aligned} A_{11}^{(k)} &= \frac{1-\nu}{(1+\nu)(1-2\nu)} \int_{-\frac{h}{2}}^{\frac{h}{2}} (z)^k E(z) dz, & A_{12}^{(k)} &= \frac{\nu}{(1+\nu)(1-2\nu)} \int_{-\frac{h}{2}}^{\frac{h}{2}} (z)^k E(z) dz \\ B_{11}^{(k)} &= \frac{1}{2(1+\nu)} \int_{-\frac{h}{2}}^{\frac{h}{2}} (z)^k E(z) dz, & \mathcal{B}_{11}^{(k)} &= \frac{l^2}{(1+\nu)} \int_{-\frac{h}{2}}^{\frac{h}{2}} (z)^k E(z) dz. \end{aligned} \tag{17}$$

#### 2.4. Equation of Motion

Reddy and Kim [24] use the principle of virtual displacements to obtain the equations of motion of GTPT. The dynamic case of the principle of virtual displacements is generalized to Hamilton’s principle [51].

$$\int_0^T (\delta\mathcal{K} - \delta\mathcal{U} - \delta\mathcal{V}) dt = 0 \tag{18}$$

where  $\delta\mathcal{K}$  is the virtual kinetic energy,  $\delta\mathcal{U}$  is the virtual strain energy, and  $\delta\mathcal{V}$  is the virtual work done by external forces. Each virtual energy terms and the virtual work are defined as

$$\delta\mathcal{K} = \int_{\Omega} \int_{-\frac{h}{2}}^{\frac{h}{2}} \rho \left( \frac{\partial u_i}{\partial t} \frac{\partial \delta u_i}{\partial t} \right) dz dx dy \tag{19}$$

$$\delta\mathcal{U} = \int_{\Omega} \int_{-\frac{h}{2}}^{\frac{h}{2}} (\sigma_{ij} \delta \epsilon_{ij} + m_{ij} \delta \chi_{ij}) dz dx dy \tag{20}$$

$$\begin{aligned} \delta\mathcal{V} = & - \left[ \int_{\Omega} \int_{-\frac{h}{2}}^{\frac{h}{2}} (\bar{f}_i \delta u_i + \bar{c}_i \delta \omega_i) dz dx dy + \int_{\Omega^+} (q_i^t \delta u_i + p_i^t \delta \omega_i) dx dy \right. \\ & \left. + \int_{\Omega^-} (q_i^b \delta u_i + p_i^b \delta \omega_i) dx dy + \int_S (\bar{t}_i \delta u_i + \bar{s}_i \delta \omega_i) dS \right] \end{aligned} \tag{21}$$

and  $\rho$  is mass density,  $\bar{f}_i$  is the body force measured per unit volume,  $\bar{c}_i$  is the body couples measured per unit volume,  $q_i^t, p_i^t, q_i^b,$  and  $p_i^b$  are distributed forces and couples on the top surface ( $\Omega^+$ ) and bottom surface ( $\Omega^-$ ), respectively,  $\bar{t}_i$  and  $\bar{s}_i$  are surface forces and couples measured per unit area acting on lateral surfaces of a plate, respectively, with the subscript  $i$  taking the values of  $x, y,$  or  $z$ . The  $\Omega$  indicates the mid surface of plates. For a rectangular plate in the Cartesian coordinate system,  $\Omega$  is define as the  $x - y$  plane at  $z = 0$ ,  $\Omega^+$  is defined at  $z = +\frac{h}{2}$ , and  $\Omega^-$  is defined at  $z = -\frac{h}{2}$ .

Substituting the generalized forces Equations (13) to (16) into Equation (20) and performing integration by parts, the equation of motion of the GTPT in terms of stress resultants are obtained as [24].

$$\begin{aligned} \delta u : & \frac{\partial M_{xx}^{(0)}}{\partial x} + \frac{\partial M_{xy}^{(0)}}{\partial y} + \frac{1}{2} \frac{\partial}{\partial y} \left( \frac{\partial \mathcal{M}_{xz}^{(0)}}{\partial x} + \frac{\partial \mathcal{M}_{yz}^{(0)}}{\partial y} \right) + F_x^{(0)} + \frac{1}{2} \frac{\partial c_z^{(0)}}{\partial y} \\ & = I_0 \ddot{u} + I_1 \ddot{\theta}_x + I_2 \ddot{\phi}_x + I_3 \ddot{\psi}_x \end{aligned} \tag{22}$$

$$\begin{aligned} \delta v : & \frac{\partial M_{xy}^{(0)}}{\partial x} + \frac{\partial M_{yy}^{(0)}}{\partial y} - \frac{1}{2} \frac{\partial}{\partial x} \left( \frac{\partial \mathcal{M}_{xz}^{(0)}}{\partial x} + \frac{\partial \mathcal{M}_{yz}^{(0)}}{\partial y} \right) + F_y^{(0)} - \frac{1}{2} \frac{\partial c_z^{(0)}}{\partial x} \\ & = I_0 \ddot{v} + I_1 \ddot{\theta}_y + I_2 \ddot{\phi}_y + I_3 \ddot{\psi}_y \end{aligned} \tag{23}$$

$$\delta \omega : \frac{\partial M_{xz}^{(0)}}{\partial x} + \frac{\partial M_{yz}^{(0)}}{\partial y} - \frac{1}{2} \frac{\partial}{\partial y} \left( \frac{\partial \mathcal{M}_{xx}^{(0)}}{\partial x} + \frac{\partial \mathcal{M}_{xy}^{(0)}}{\partial y} \right) + \frac{1}{2} \frac{\partial}{\partial x} \left( \frac{\partial \mathcal{M}_{yy}^{(0)}}{\partial y} + \frac{\partial \mathcal{M}_{xy}^{(0)}}{\partial x} \right)$$

$$+ F_z^{(0)} + \frac{1}{2} \left( \frac{\partial c_y^{(0)}}{\partial x} - \frac{\partial c_x^{(0)}}{\partial y} \right) = I_0 \ddot{w} + I_1 \ddot{\theta}_z + I_2 \ddot{\phi}_z \tag{24}$$

$$\begin{aligned} \delta \theta_x : & \frac{\partial M_{xx}^{(1)}}{\partial x} + \frac{\partial M_{xy}^{(1)}}{\partial y} - M_{xz}^{(0)} + \frac{1}{2} \left( \frac{\partial \mathcal{M}_{xy}^{(0)}}{\partial x} + \frac{\partial \mathcal{M}_{yy}^{(0)}}{\partial y} - \frac{\partial \mathcal{M}_{zz}^{(0)}}{\partial y} \right) + \frac{1}{2} \frac{\partial}{\partial y} \left( \frac{\partial \mathcal{M}_{xz}^{(1)}}{\partial x} + \frac{\partial \mathcal{M}_{yz}^{(1)}}{\partial y} \right) \\ & + F_x^{(1)} + \frac{1}{2} c_y^{(0)} + \frac{1}{2} \frac{\partial c_z^{(1)}}{\partial y} = I_1 \ddot{u} + I_2 \ddot{\theta}_x + I_3 \ddot{\phi}_x + I_4 \ddot{\psi}_x \end{aligned} \tag{25}$$

$$\begin{aligned} \delta \theta_y : & \frac{\partial M_{xy}^{(1)}}{\partial x} + \frac{\partial M_{yy}^{(1)}}{\partial y} - M_{yz}^{(0)} - \frac{1}{2} \left( \frac{\partial \mathcal{M}_{xx}^{(0)}}{\partial x} + \frac{\partial \mathcal{M}_{xy}^{(0)}}{\partial y} - \frac{\partial \mathcal{M}_{zz}^{(0)}}{\partial x} \right) - \frac{1}{2} \frac{\partial}{\partial x} \left( \frac{\partial \mathcal{M}_{xz}^{(1)}}{\partial x} + \frac{\partial \mathcal{M}_{yz}^{(1)}}{\partial y} \right) \\ & + F_y^{(1)} - \frac{1}{2} c_x^{(0)} - \frac{1}{2} \frac{\partial c_z^{(1)}}{\partial x} = I_1 \ddot{v} + I_2 \ddot{\theta}_y + I_3 \ddot{\phi}_y + I_4 \ddot{\psi}_y \end{aligned} \tag{26}$$

$$\begin{aligned} \delta \theta_z : & \frac{\partial M_{xz}^{(1)}}{\partial x} + \frac{\partial M_{yz}^{(1)}}{\partial y} - M_{zz}^{(0)} - \frac{1}{2} \frac{\partial}{\partial y} \left( \frac{\partial \mathcal{M}_{xx}^{(1)}}{\partial x} + \frac{\partial \mathcal{M}_{xy}^{(1)}}{\partial y} \right) + \frac{1}{2} \frac{\partial}{\partial x} \left( \frac{\partial \mathcal{M}_{yy}^{(1)}}{\partial y} + \frac{\partial \mathcal{M}_{xy}^{(1)}}{\partial x} \right) \\ & + \frac{1}{2} \left( \frac{\partial \mathcal{M}_{xz}^{(0)}}{\partial y} - \frac{\partial \mathcal{M}_{yz}^{(0)}}{\partial x} \right) + F_z^{(1)} + \frac{1}{2} \left( \frac{\partial c_y^{(1)}}{\partial x} - \frac{\partial c_x^{(1)}}{\partial y} \right) = I_1 \ddot{w} + I_2 \ddot{\theta}_z + I_3 \ddot{\phi}_z \end{aligned} \tag{27}$$

$$\begin{aligned} \delta \phi_x : & \frac{\partial M_{xx}^{(2)}}{\partial x} + \frac{\partial M_{xy}^{(2)}}{\partial y} - 2M_{xz}^{(1)} + \left( \frac{\partial \mathcal{M}_{xy}^{(1)}}{\partial x} + \frac{\partial \mathcal{M}_{yy}^{(1)}}{\partial y} - \frac{\partial \mathcal{M}_{zz}^{(1)}}{\partial y} - \mathcal{M}_{yz}^{(0)} \right) \\ & + \frac{1}{2} \frac{\partial}{\partial y} \left( \frac{\partial \mathcal{M}_{xz}^{(2)}}{\partial x} + \frac{\partial \mathcal{M}_{yz}^{(2)}}{\partial y} \right) + F_x^{(2)} + \frac{1}{2} c_y^{(1)} + \frac{1}{2} \frac{\partial c_z^{(2)}}{\partial y} = I_2 \ddot{u} + I_3 \ddot{\theta}_x + I_4 \ddot{\phi}_x + I_5 \ddot{\psi}_x \end{aligned} \tag{28}$$

$$\begin{aligned} \delta \phi_y : & \frac{\partial M_{xy}^{(2)}}{\partial x} + \frac{\partial M_{yy}^{(2)}}{\partial y} - 2M_{yz}^{(1)} - \left( \frac{\partial \mathcal{M}_{xx}^{(1)}}{\partial x} + \frac{\partial \mathcal{M}_{xy}^{(1)}}{\partial y} - \frac{\partial \mathcal{M}_{zz}^{(1)}}{\partial x} - \mathcal{M}_{xz}^{(0)} \right) \\ & - \frac{1}{2} \frac{\partial}{\partial x} \left( \frac{\partial \mathcal{M}_{xz}^{(2)}}{\partial x} + \frac{\partial \mathcal{M}_{yz}^{(2)}}{\partial y} \right) + F_y^{(2)} - \frac{1}{2} c_x^{(1)} - \frac{1}{2} \frac{\partial c_z^{(2)}}{\partial x} = I_2 \ddot{v} + I_3 \ddot{\theta}_y + I_4 \ddot{\phi}_y + I_5 \ddot{\psi}_y \end{aligned} \tag{29}$$

$$\begin{aligned} \delta \phi_z : & \frac{\partial M_{xz}^{(2)}}{\partial x} + \frac{\partial M_{yz}^{(2)}}{\partial y} - 2M_{zz}^{(1)} - \frac{1}{2} \frac{\partial}{\partial y} \left( \frac{\partial \mathcal{M}_{xx}^{(2)}}{\partial x} + \frac{\partial \mathcal{M}_{xy}^{(2)}}{\partial y} \right) + \frac{1}{2} \frac{\partial}{\partial x} \left( \frac{\partial \mathcal{M}_{yy}^{(2)}}{\partial y} + \frac{\partial \mathcal{M}_{xy}^{(2)}}{\partial x} \right) \\ & + \frac{\partial \mathcal{M}_{xz}^{(1)}}{\partial y} - \frac{\partial \mathcal{M}_{yz}^{(1)}}{\partial x} + F_z^{(2)} + \frac{1}{2} \left( \frac{\partial c_y^{(2)}}{\partial x} - \frac{\partial c_x^{(2)}}{\partial y} \right) = I_2 \ddot{w} + I_3 \ddot{\theta}_z + I_4 \ddot{\phi}_z \end{aligned} \tag{30}$$

$$\begin{aligned} \delta \psi_x : & \frac{\partial M_{xx}^{(3)}}{\partial x} + \frac{\partial M_{xy}^{(3)}}{\partial y} - 3M_{xz}^{(2)} + \frac{3}{2} \left( \frac{\partial \mathcal{M}_{xy}^{(2)}}{\partial x} + \frac{\partial \mathcal{M}_{yy}^{(2)}}{\partial y} - \frac{\partial \mathcal{M}_{zz}^{(2)}}{\partial y} - 2\mathcal{M}_{yz}^{(1)} \right) \\ & + \frac{1}{2} \frac{\partial}{\partial y} \left( \frac{\partial \mathcal{M}_{xz}^{(3)}}{\partial x} + \frac{\partial \mathcal{M}_{yz}^{(3)}}{\partial y} \right) + F_x^{(3)} + \frac{3}{2} c_y^{(2)} + \frac{1}{2} \frac{\partial c_z^{(3)}}{\partial y} = I_3 \ddot{u} + I_4 \ddot{\theta}_x + I_5 \ddot{\phi}_x + I_6 \ddot{\psi}_x \end{aligned} \tag{31}$$

$$\begin{aligned} \delta \psi_y : & \frac{\partial M_{xy}^{(3)}}{\partial x} + \frac{\partial M_{yy}^{(3)}}{\partial y} - 3M_{yz}^{(2)} - \frac{3}{2} \left( \frac{\partial \mathcal{M}_{xx}^{(2)}}{\partial x} + \frac{\partial \mathcal{M}_{xy}^{(2)}}{\partial y} - \frac{\partial \mathcal{M}_{zz}^{(2)}}{\partial x} - 2\mathcal{M}_{xz}^{(1)} \right) \\ & - \frac{1}{2} \frac{\partial}{\partial x} \left( \frac{\partial \mathcal{M}_{xz}^{(3)}}{\partial x} + \frac{\partial \mathcal{M}_{yz}^{(3)}}{\partial y} \right) + F_y^{(3)} - \frac{3}{2} c_x^{(2)} - \frac{1}{2} \frac{\partial c_z^{(3)}}{\partial x} = I_3 \ddot{v} + I_4 \ddot{\theta}_y + I_5 \ddot{\phi}_y + I_6 \ddot{\psi}_y \end{aligned} \tag{32}$$

where  $F_{\xi}^{(i)} = \bar{f}_{\xi}^{(i)} + \left(\frac{h}{2}\right)^i \left[ q_{\xi}^t + (-1)^i q_{\xi}^b \right]$ ,  $\bar{f}^i = \int_{-\frac{h}{2}}^{\frac{h}{2}} (z)^i f_{\xi} dz$ ,  $c_{\xi}^{(i)} = \int_{-\frac{h}{2}}^{\frac{h}{2}} (z)^i \bar{c}_{\xi} dz$  for  $i = 0, 1, 2, 3$  and  $\xi = x, y, z$ . The superposed dot are used to indicate the time derivative, hence  $\ddot{u} = \partial^2 u / \partial t^2$ . The mass resultants  $I_0, I_1, \dots, I_6$  are defined as

$$I_i = \int_{-h/2}^{h/2} \rho(z)^i dz, \quad i = 0, 1, \dots, 6 \tag{33}$$

The equations of motion for GTPT in terms of generalized displacements can be found in the references [24,25].

### 3. Solution Procedure

Navier solution technique is applied to obtain analytical solutions to static bending, free vibration and buckling problems for a simply supported rectangular FGPM plate. The boundary conditions of the simply supported plate are demonstrated in Figure 2a. Figure 2b shows the cross-sectional view of typical FGP plate used in this study (e.g., Type 3 is illustrated in Figure 2b). Also,  $x - z$  cross section is identical to  $y - z$  cross section of the plates.

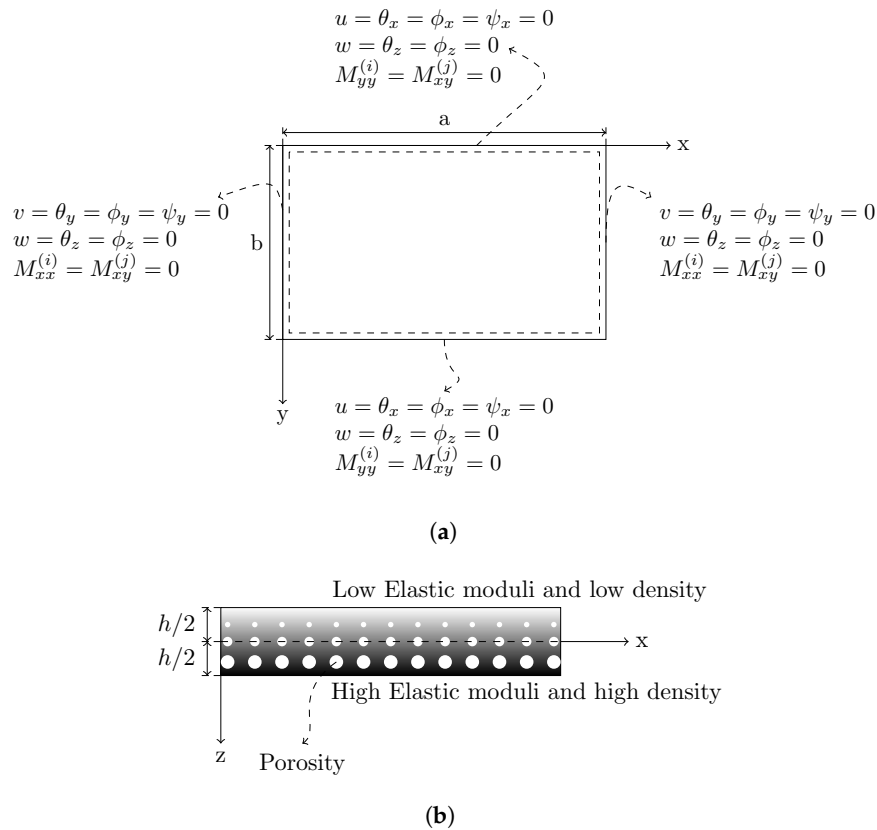


**Figure 2.** Boundary conditions of the simply supported plate [50] (where  $i = 0, 1, 2, 3$  and  $j = 0, 1, 2$ ) (a) and the cross-section of the FGPM plate (Type 3) (b).

To employ the Navier solution technique, the generalized displacements ( $u, v, w, \theta_x, \theta_y, \theta_z, \phi_x, \phi_y, \phi_z, \psi_x,$  and  $\psi_y$ ) and applied load ( $q_z$ ) are expanded in double trigonometric series which are selected to satisfy the boundary conditions of the simply supported plate problem. The following double trigonometric series are used to expand the generalized displacements

$$\begin{aligned}
 u(x, y, z, t) &= \sum_{m=1}^{\infty} \sum_{n=1}^{\infty} U_{mn}(t) \cos(\alpha x) \sin(\beta y) \\
 v(x, y, z, t) &= \sum_{m=1}^{\infty} \sum_{n=1}^{\infty} V_{mn}(t) \sin(\alpha x) \cos(\beta y) \\
 w(x, y, z, t) &= \sum_{m=1}^{\infty} \sum_{n=1}^{\infty} W_{mn}(t) \sin(\alpha x) \sin(\beta y) \\
 \theta_x(x, y, z, t) &= \sum_{m=1}^{\infty} \sum_{n=1}^{\infty} \Theta_{xmn}(t) \cos(\alpha x) \sin(\beta y) \\
 \theta_y(x, y, z, t) &= \sum_{m=1}^{\infty} \sum_{n=1}^{\infty} \Theta_{ymn}(t) \sin(\alpha x) \cos(\beta y)
 \end{aligned}$$

$$\begin{aligned}
 \theta_z(x, y, z, t) &= \sum_{m=1}^{\infty} \sum_{n=1}^{\infty} \Theta_{zmn}(t) \sin(\alpha x) \sin(\beta y) \\
 \phi_x(x, y, z, t) &= \sum_{m=1}^{\infty} \sum_{n=1}^{\infty} \Phi_{xmn}(t) \cos(\alpha x) \sin(\beta y) \\
 \phi_y(x, y, z, t) &= \sum_{m=1}^{\infty} \sum_{n=1}^{\infty} \Phi_{ymn}(t) \sin(\alpha x) \cos(\beta y) \\
 \phi_z(x, y, z, t) &= \sum_{m=1}^{\infty} \sum_{n=1}^{\infty} \Phi_{zmn}(t) \sin(\alpha x) \sin(\beta y) \\
 \psi_x(x, y, z, t) &= \sum_{m=1}^{\infty} \sum_{n=1}^{\infty} \Psi_{xmn}(t) \cos(\alpha x) \sin(\beta y) \\
 \psi_y(x, y, z, t) &= \sum_{m=1}^{\infty} \sum_{n=1}^{\infty} \Psi_{ymn}(t) \sin(\alpha x) \cos(\beta y)
 \end{aligned} \tag{34}$$

where  $\alpha = \frac{m\pi}{a}$ ,  $\beta = \frac{n\pi}{b}$ . The generalized displacement coefficients ( $U_{mn}$ ,  $V_{mn}$ ,  $W_{mn}$ ,  $\Theta_{xmn}$ ,  $\Theta_{ymn}$ ,  $\Theta_{zmn}$ ,  $\Phi_{xmn}$ ,  $\Phi_{ymn}$ ,  $\Phi_{zmn}$ ,  $\Psi_{xmn}$ , and  $\Psi_{ymn}$ ) are treated as time independent variables for static bending and buckling problems.

For the static bending problem, a uniformly distributed transverse load  $q_z$  is defined as acting to the top surface of the plate, which is also expanded in double trigonometric series in Equation (35). Because  $q_z$  is assumed as an uniformly distributed load, the coefficient for the applied force is simplified as shown in Equation (36).

$$q_z = \sum_{m=1}^{\infty} \sum_{n=1}^{\infty} Q_{mn}(t) \sin(\alpha x) \sin(\beta y) \tag{35}$$

where

$$Q_{mn} = \frac{4}{ab} \int_0^a \int_0^b q_z \sin(\alpha x) \sin(\beta y) dx dy = \frac{16q_0}{mn\pi^2} \tag{36}$$

where  $q_0$  is the magnitude of the applied uniformly distributed load.

After substituting these expanded forms into the equation of motions (22) to (32), the algebraic system of equations are obtained for static bending problem as

$$[C]_{mn} \{\Delta\}_{mn} = \{F\}_{mn} \tag{37}$$

where  $[C]$  is the 11 by 11 coefficient matrix whose expanded form can be found in the Kim and Reddy’s study [25],  $\{\Delta\}$  is the vector of generalized displacements, and  $\{F\}$  is the force vector given in Equation (38).

$$\{\Delta\}_{mn} = \begin{pmatrix} U_{mn} \\ V_{mn} \\ W_{mn} \\ \Theta_{xmn} \\ \Theta_{ymn} \\ \Theta_{zmn} \\ \Phi_{xmn} \\ \Phi_{ymn} \\ \Phi_{zmn} \\ \Psi_{xmn} \\ \Psi_{ymn} \end{pmatrix}, \quad \{F\}_{mn} = \begin{pmatrix} 0 \\ 0 \\ Q_{mn} \\ 0 \\ 0 \\ \frac{h}{2} Q_{mn} \\ 0 \\ 0 \\ \frac{h^2}{4} Q_{mn} \\ 0 \\ 0 \end{pmatrix} \tag{38}$$

Equation (37) is solved for each  $m = 1, 3, 5, \dots$  and  $n = 1, 3, 5, \dots$  in order to find generalized displacements  $\{\Delta\}$ . Then, generalized displacements for each  $m$  and  $n$  are inserted into the double

trigonometric form of displacements given in Equation (34) to obtain displacements  $u, v, w, \theta_x, \theta_y, \theta_z, \phi_x, \phi_y, \phi_z, \psi_x,$  and  $\psi_y$ .

In the case of free vibration analysis, the time dependent generalized displacements in Equation (34) are assumed as

$$\{\Delta(t)\}_{mn} = e^{-i\omega t} \{\Delta\}_{mn} \tag{39}$$

where  $\omega$  is the natural frequency. By substituting Equations (34) and (39) into the equation of motion, we setup the eigenvalue problem to determine eigenfrequencies:

$$\{[C]_{mn} - \omega_{mn}^2 [M]_{mn}\} \{\Delta\}_{mn} = \{0\} \tag{40}$$

where  $[C]$  is the coefficient matrix which is the same as the one in the bending analysis,  $[M]$  is the matrix of inertias (please see [25]), and  $\Delta$  is the vector of generalized displacements. The free vibration analysis of simply supported square FGPM plate is performed by solving Equation (40). The fundamental frequencies are then obtained when  $m = 1$  and  $n = 1$ .

For buckling analysis, the simply supported plate is assumed under in-plane compressive forces acting on  $x$  and  $y$  edges which are  $\hat{N}_{xx}$  and  $\hat{N}_{yy}$ , respectively. Then, additional  $\hat{N}_{xx} \frac{\partial^2 w}{\partial x^2} + \hat{N}_{yy} \frac{\partial^2 w}{\partial y^2}$  terms are inserted in right hand side of Equation (24). The following system of equations is obtained to find the buckling loads  $N_0$ ;

$$\{[C]_{mn} - [N]_{mn}\} \{\Delta\}_{mn} = \{0\} \tag{41}$$

where  $[N]$  is the matrix with only nonzero element is  $N_{33} = N_0(\alpha^2 + k\beta^2), k = \frac{\hat{N}_{yy}}{\hat{N}_{xx}}$ . After performing a static condensation to Equation (41) and setting  $m = 1$  and  $n = 1$ , the critical buckling load is found as

$$N_0 = \frac{1}{\alpha^2 + k\beta^2} \left( C_{0303} - \begin{matrix} \begin{matrix} C_{0301} \\ C_{0302} \\ C_{0304} \\ C_{0305} \\ \vdots \\ C_{0310} \\ C_{0311} \end{matrix}^T \\ [ \bar{C} ] \begin{matrix} C_{0103} \\ C_{0203} \\ C_{0403} \\ C_{0503} \\ \vdots \\ C_{1003} \\ C_{1103} \end{matrix} \end{matrix} \right). \tag{42}$$

where

$$[ \bar{C} ] = \begin{bmatrix} C_{0101} & C_{0102} & C_{0104} & C_{0105} & \cdots & C_{0110} & C_{0111} \\ C_{0201} & C_{0202} & C_{0204} & C_{0205} & \cdots & C_{0210} & C_{0211} \\ C_{0401} & C_{0402} & C_{0404} & C_{0405} & \cdots & C_{0410} & C_{0411} \\ C_{0501} & C_{0502} & C_{0504} & C_{0505} & \cdots & C_{0510} & C_{0511} \\ \vdots & \vdots & \vdots & \vdots & \ddots & \vdots & \vdots \\ C_{1001} & C_{1002} & C_{1004} & C_{1005} & \cdots & C_{1010} & C_{1011} \\ C_{1101} & C_{1102} & C_{1104} & C_{1105} & \cdots & C_{1110} & C_{1111} \end{bmatrix}^{-1}.$$

In the numerical solutions, it is assumed that the square FGPM plate is under the same amount of compressive force acting in  $x$  and  $y$  edges (i.e., their ratio,  $k = 1$ ).

#### 4. Numerical Results and Discussions

Numerical examples of the analytical solutions given in the previous section are obtained using the material properties and the dimensions of the functionally graded plate from the study of Kim and Reddy [25]. The dimensions of functionally graded plate in Figure 2 are  $a = 20h, b = 20h,$  and  $h = 17.6 \times 10^{-6}$  m. The moduli and mass densities of two constituents are  $E_t = 14.4$  GPa,  $E_b = 1.44$  GPa,  $\rho_t = 12.2 \times 10^3$  kg/m, and  $\rho_b = 1.22 \times 10^3$  kg/m with the Poisson ratio ( $\nu$ ) of 0.38.

4.1. Verification

To show the consistency of the present study with the literature, the static bending, free vibration and buckling results are compared with the results of the previously published papers. One of the selected paper is based on the general third order plate theory [25], a generalized third order shear deformation theory (TSDT) for plates, for functionally graded plates without considering the porosity effect. The second paper has the same porosity distributions with the current study; however, it is based on classical plate theory (CPT) and first order shear deformation theory (FSDT) [49]. As can be seen from Figure 3, the present study shows good agreement with the previous studies. For non-porous cases, the current results and the Kim’s results are identical because they both uses the GTPT. On the other hand, the comparison with the second paper shows a small deviation resulted from the differences in the applied theories.

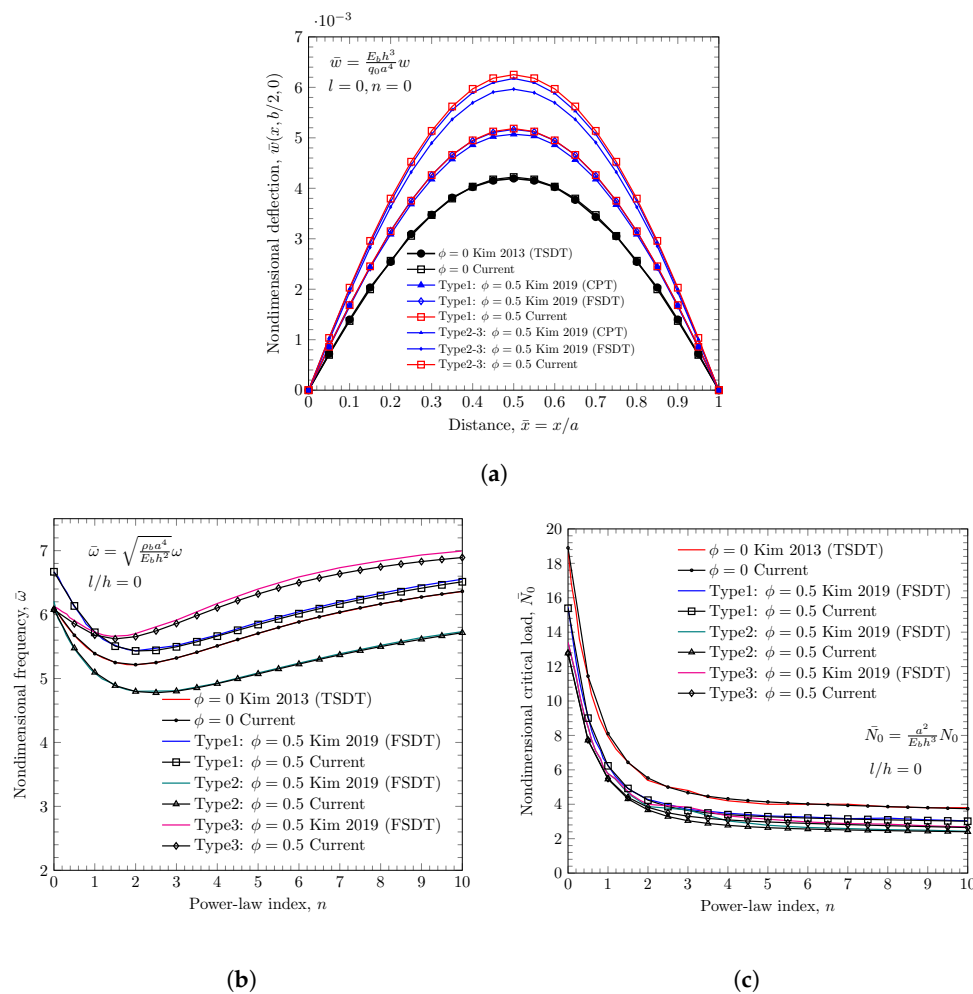


**Figure 3.** Comparisons of the non-dimensional deflection,  $\bar{w}(x, \frac{b}{2}, 0)$  (a), the non-dimensional fundamental frequency,  $\bar{\omega}$  (b), and the non-dimensional critical buckling load,  $\bar{N}_0$  (c).

4.2. Static Bending

In the static bending problem, the uniformly distributed load of  $q_0 = 1 \text{ N/m}^2$  is applied to the top surface of the simply supported FGP plate. The generalized displacements and the applied load are expanded in double trigonometric series which are given in Equations (34) and (35) up to  $m = 31$  and  $n = 31$  terms. Then, the system equation given in Equation (37) is solved.

The non-dimensional transverse deflections at  $y = b/2$  along  $x$  for porous plates without variation of material constituents are shown in Figure 4a. The length scale parameter effect is also neglected to see

the effect of porosity variations clearly. Because the power-law index is set to zero (see Equation (11)), the plate consists of a single material which is the top surface material. As expected, while the porosity of the plate increases, the bending stiffness of the plate decreases. Hence, larger deflection values are obtained for more porous plates. It is important to remind that although distribution types are different, the total porosity volume of the plates result from them are the same. Hence, a reasonable comparison of the type of porosity distribution can be conducted. Another important point is that in the case of Type 1 distribution of homogeneous plate, we have symmetric variation of the porosity distribution about the mid-plane of the plate, which decrease the effect of coupling terms in the coefficient matrix given in Equation (37). On the other hand, this is not the case for Type 2 and Type 3 distributions even for the  $n = 0$  case.

Figure 4 shows the center deflections of simply supported homogeneous plates with various porosity variations and FGM plates with various power-law indices. Figure 4a clearly shows that the porosity distribution types result in different bending rigidity; although they have the same amount of porosity values. The plate with Type 1 distribution are stiffer than the those with Type 2 and 3 with same porosity. The reason is that Type 1 distribution results in high porosity values at the mid-plate and the very low values as one moves through the top and the bottom surfaces (please see Figure 1a). Furthermore, the transverse deflection values for Type 2 and 3 are the same, because the plate is homogeneous and the resultant material property of them are the same. The only difference is that porous volume increases from top surface to the bottom for Type 2, while it increases from bottom to the top surface of the plate for the case of Type 3. It makes no difference in terms of bending rigidity for homogeneous plates.

Figure 4b shows the nondimensional transverse deflection along  $x$  while  $y = b/2$  for functionally graded porous plate without including the length scale parameter. High deflection values are obtained as the power-law index increases for each distribution. The reason is that while the power-law index increases, the material property distributions become highly asymmetric and therefore the effects of coupling terms come into the picture and start to influence the results dramatically. Also for larger values of power-law index, the deflections of Type 2 and Type 3 start to deviate from each other. For example, when  $n = 5$ , Type 2 shows the higher transverse deflections than Type 3. Because Type 2 is the most sensitive porosity distribution type for the given material configuration (i.e.,  $E_t/E_b = 10$ ) and the most influenced type by the effect of power-law index. On the other hand, Type 3 is least effected one by the change of  $n$ .

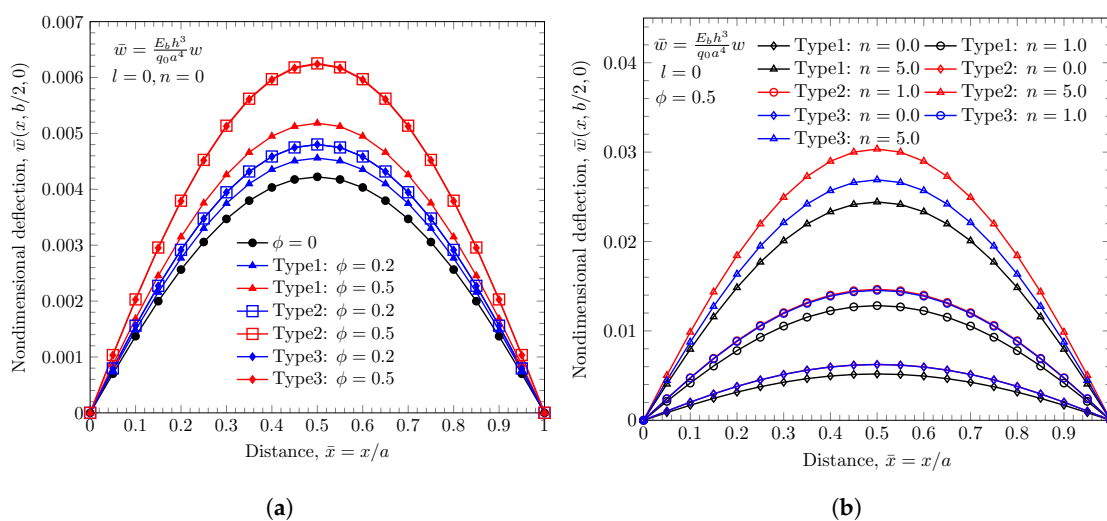
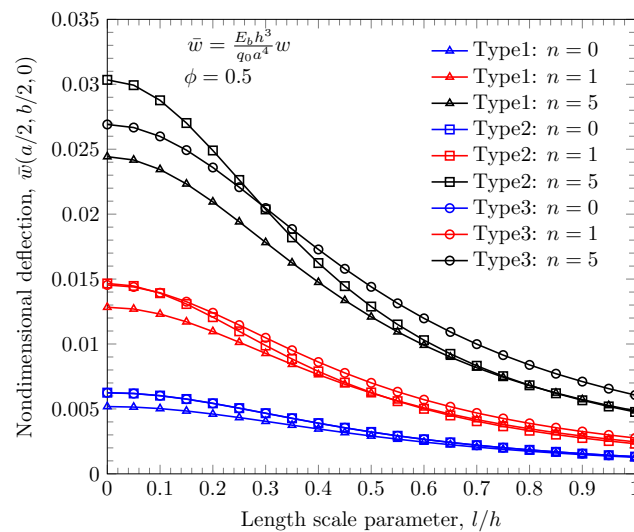


Figure 4. Non-dimensional deflection  $\bar{w}(x, \frac{b}{2}, 0)$  of homogeneous plate with different porosity distributions (a) and FGM plate with various power-law index,  $n$  (b).

The effect of the length scale parameter is presented in Figure 5 for FGPM plate. This figure clearly shows that the length scale parameter has an important contribution to capture the deformation behavior of the micro plates. Indeed, to find the more accurate results from the numerical analysis, the length scale factor for the micro-plates should be determined first. Regardless of the porosity and the variations in the constituents, the plate stiffness increases as the length parameter increases. For a porous plate without material variation ( $n = 0$ ), the effect of porosity distribution type becomes negligible for length scale parameter values higher than  $0.6h$ , because the influence of the length scale parameter has a dominant effect in this regime. Similarly, for functionally graded plates ( $n \neq 0$ ), the central deflection values obtained from Type 1 and 2 become quite similar for large values of length scale parameter (larger than  $0.6h$ ). On the other hand, the effect of length scale parameter is not much dominant for Type 3 compared to Type 1 and 2. Moreover, for large values of power-law index and the small length parameter, Type 2 results high transverse deflection values as compared to Type 1 and 3, due to differences in the effects of coupling terms.

For an illustration of stress variations of higher order shear deformation theory, the bending stresses and transverse shear stresses of the porosity distribution Type 1 are presented in Figure 6. The black line without a marker shows the variations of stresses in homogeneous materials ( $n = 0$ ). It clearly shows that the distribution of bending stress of higher order plate theory is similar to ones obtained from the classical and first order shear deformation theory (i.e., linear variation of bending stress) but the distribution of transverse shear stresses take the form of a parabolic variation that cannot be presented by the classical and the first order shear deformation theory. Also, Figure 6 shows effects of porosity distribution and length scale parameters. The stress variations are highly affected by the variations of material properties in Figure 1b.



**Figure 5.** Non-dimensional central deflection  $\bar{w} \left( \frac{a}{2}, \frac{b}{2}, 0 \right)$  versus length scale parameter  $l/h$  along a FGM simply supported plate with constant porosity,  $\phi = 0.5$  and various power law index  $n$ .

### 4.3. Free Vibration

The fundamental frequencies of the functionally graded porous plates are obtained by solving Equation (40) for  $m = 1$  and  $n = 1$ .

Figure 7 shows the nondimensional fundamental frequencies versus porosity distributions for various power-law indices without including length scale parameter. The porous plate without material variation, i.e.,  $n = 0$ , the natural frequencies of the plate with Type 1 porosity distribution show higher values compared the ones with Type 2 and 3 porosity distributions. Although the total mass of the plates decreases same amount as the porosity increases regardless of the distribution types, Type 2 and 3 result a decrease in natural frequency values as the porosity increases because the stiffness of the plate is

significantly degraded in the case of Type 2 and 3. For the FGPM plates with nonzero power-law index, Type 1 and 3 distribution show increase in natural frequency values as the porosity increases. However, Type 2 exhibits the reverse behavior because of the strong contribution coming from the coupling terms which are resulted from the heterogeneity in both porosity distribution and the enhancement in material variation (the density of the plate porosity is very small above the mid-plane section in the case of Type 2 distribution and  $E_t/E_b = 10, \rho_t/\rho_b = 10$ ). The variation of the nondimensional form of fundamental frequencies with varying power-law index and the length scale parameter is presented in Figure 8. The length scale parameter causes significant change in fundamental frequencies of the plates because the stiffening effect in small scale structures is captured by the length scale parameter. Although Type 1 and 3 result higher frequencies compared to the non-porous plate, the frequency values obtained from Type 2 distribution are lower than both non-porous plate and the plate with porosity distribution of Type 1 and 3. As stated before, the reason is that Type 2 is the most effected distribution types by the heterogeneity (with high Elastic modulus and low porosity density at the top sections and reverse at the bottom sections of the plate) and hence this causes high impact of coupling terms which change the behavior significantly.

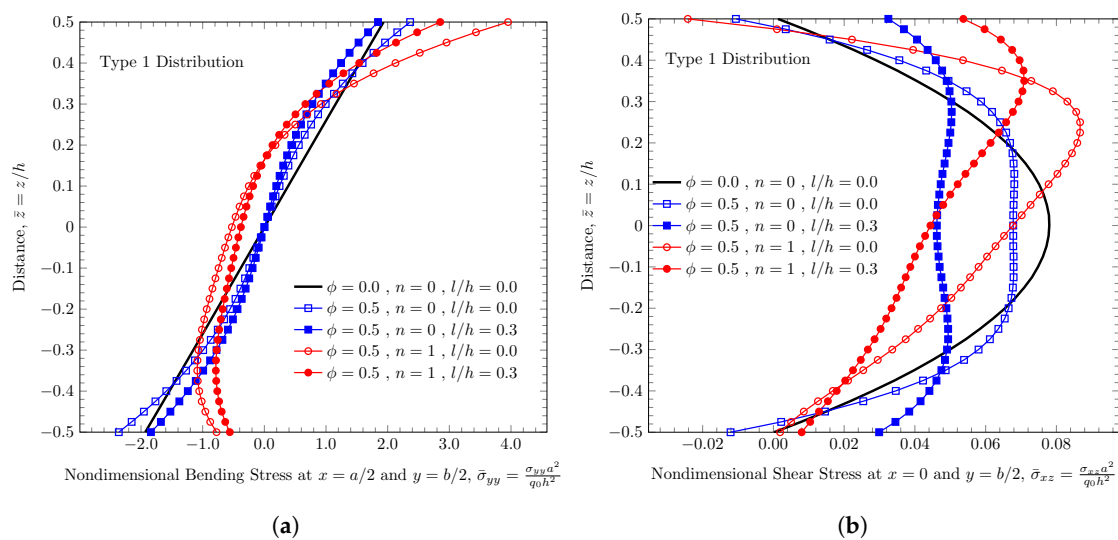


Figure 6. Bending stresses ( $\bar{\sigma}_{yy}$ ) distribution (a) and transverse shear stresses ( $\bar{\sigma}_{xz}$ ) distribution (b) through plate thickness.

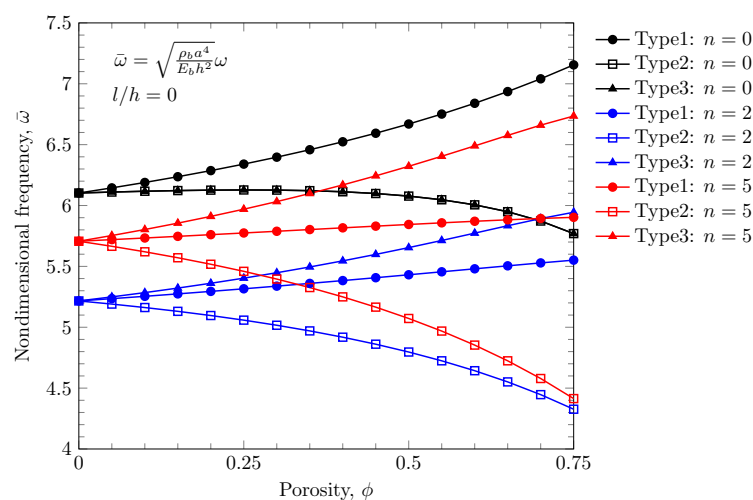
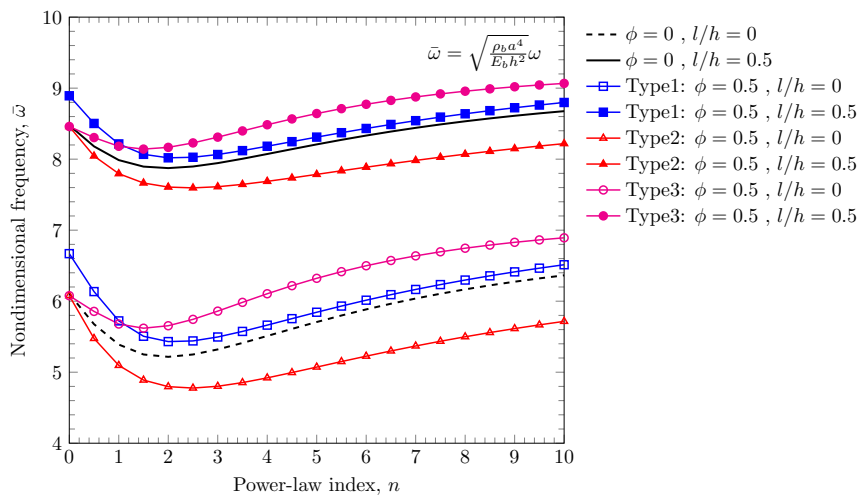


Figure 7. Non-dimensional fundamental frequency,  $\bar{\omega}$  versus porosity values,  $\phi$  with zero length scale parameter  $l/h = 0$ .



**Figure 8.** Non-dimensional fundamental frequency,  $\bar{\omega}$  versus power-law index,  $n$ .

#### 4.4. Buckling

The critical buckling load is obtained by solving Equation (42) for the functionally graded porous plate subjected to in-plane compressive forces.

Figure 9 shows the variation of non-dimensional critical buckling load with porosity values for FGPM square plate. It is clearly shown that as the power-law index increases the critical buckling load decreases, which makes the plate susceptible to buckling failures. This is also valid for the porosity factor. As expected, as the porosity of the material increases, plate become softer. Also, Type 1 distribution results in stiffer behavior against buckling regardless of the power-law index.

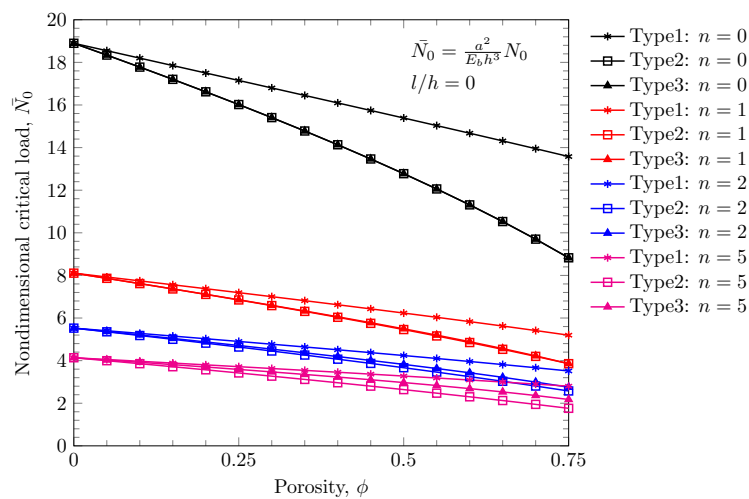


**Figure 9.** Non-dimensional critical buckling load,  $\bar{N}_0$  versus porosity values,  $\phi$  with zero length scale parameter  $l/h = 0$ .

The results of the investigation of the effect of length scale parameter for FGPM are given from Figure 10. To examine the effect of the different porosity distribution types, the porosity value is kept constant as 0.5. As in the case of bending and the free vibration analysis, the stiffness of the plates increase as the length scale parameter increases. On the other hand, the differences in the porosity variation and the enhanced modulus for the top portion of the plate cause deviations and different trends for each porosity distribution.

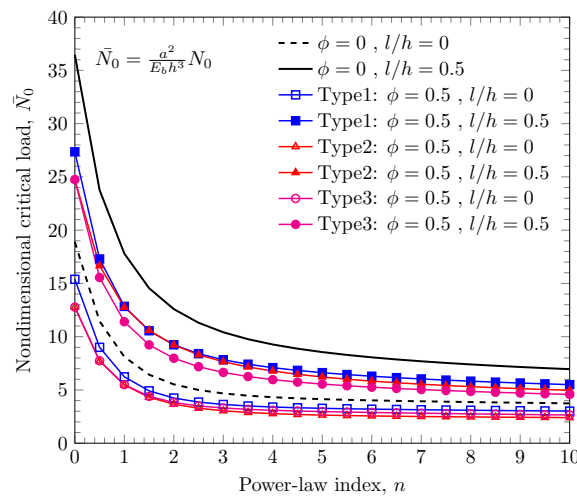


Figure 10. Non-dimensional critical buckling load,  $\bar{N}_0$  versus power-law index,  $n$ .

### 5. Conclusions

Static bending, free vibration and buckling analysis of the functionally graded porous micro-plates are conducted using general third order plate theory (GTPT) developed by Reddy and Kim [24] and solutions are obtained using Navier’s solution technique. The effect of the material length scale factor and material property variation through the plate thickness direction are included while using the third order plate theory. Three different porosity distributions are used in the analysis and the effects of porosity variations are investigated. In the numerical problems, the elastic modulus and density of the plate have power-law distribution through the thickness while keeping top material is stiffer and denser ( $E_t/E_b = 10$  and  $\rho_t/\rho_b = 10$ ).

The results of the bending, free vibration and the buckling problems show that each distribution has different responses due to effect of coupling terms resulted from the heterogeneity of the material properties and symmetric or/and asymmetric variation of porosity. In general, because of the assumption that  $E_t/E_b = 10$ , the plate becomes softer as the power-law index increases. Also, the material length scale parameter has a strong effect which makes the plate stiffer. The numerical solutions of this study is limited to rectangular simply supported plate due to the limitation of Navier solution technique.

**Author Contributions:** Conceptualization, S.C., J.K., and H.T.; methodology, J.K.; software, S.C. and J.K.; validation, S.C. and J.K.; formal analysis, S.C.; investigation, S.C.; resources, J.K. and H.T.; data curation, S.C.; writing—original draft preparation, S.C.; writing—review and editing, J.K. and H.T.; visualization, S.C.; supervision, J.K. and H.T.; project administration, J.K. and H.T.; funding acquisition, H.T.

**Funding:** This research was funded by Western Michigan University.

**Acknowledgments:** The authors gratefully acknowledges the support of Western Michigan University through research start-up fund.

**Conflicts of Interest:** The authors declare no conflict of interest.

### References

1. Bhushan, B. Nanotribology and nanomechanics of MEMS/NEMS and BioMEMS/BioNEMS materials and devices. In *Nanotribology and Nanomechanics: An Introduction*, 4th ed.; Springer: Berlin/Heidelberg, Germany, 2017.
2. Fleck, N.A.; Muller, G.M.; Ashby, M.F.; Hutchinson, J.W. Strain gradient plasticity: Theory and experiment. *Acta Metall. Mater.* **1994**, *42*, 475–487. [[CrossRef](#)]
3. Lam, D.C.; Yang, F.; Chong, A.C.; Wang, J.; Tong, P. Experiments and theory in strain gradient elasticity. *J. Mech. Phys. Solids* **2003**, *51*, 1477–1508. [[CrossRef](#)]

4. Mcfarland, A.W.; Colton, J.S. Role of material microstructure in plate stiffness with relevance to microcantilever sensors. *J. Micromech. Microeng.* **2005**, *15*, 1060–1067. [[CrossRef](#)]
5. Motz, C.; Schöberl, T.; Pippin, R. Mechanical properties of micro-sized copper bending beams machined by the focused ion beam technique. *Acta Mater.* **2005**, *53*, 4269–4279. [[CrossRef](#)]
6. Demir, E.; Raabe, D.; Roters, F. The mechanical size effect as a mean-field breakdown phenomenon: Example of microscale single crystal beam bending. *Acta Mater.* **2010**, *58*, 1876–1886. [[CrossRef](#)]
7. Ke, L.L.; Wang, Y.S. Size effect on dynamic stability of functionally graded microbeams based on a modified couple stress theory. *Compos. Struct.* **2011**, *93*, 342–350. [[CrossRef](#)]
8. Liu, D.; He, Y.; Dunstan, D.J.; Zhang, B.; Gan, Z.; Hu, P.; Ding, H. Toward a further understanding of size effects in the torsion of thin metal wires: An experimental and theoretical assessment. *Int. J. Plast.* **2013**, *41*, 30–52. [[CrossRef](#)]
9. Chen, D.; Yang, J.; Kitipornchai, S. Elastic buckling and static bending of shear deformable functionally graded porous beam. *Compos. Struct.* **2015**, *133*, 54–61. [[CrossRef](#)]
10. Toupin, R.A. Elastic materials with couple-stresses. *Arch. Ration. Mech. Anal.* **1962**, *11*, 385–414. [[CrossRef](#)]
11. Mindlin, R.D.; Tiersten, H.F. Effects of couple-stresses in linear elasticity. *Arch. Ration. Mech. Anal.* **1962**, *11*, 415–448. [[CrossRef](#)]
12. Yang, F.; Chong, A.C.; Lam, D.C.; Tong, P. Couple stress based strain gradient theory for elasticity. *Int. J. Solids Struct.* **2002**, *39*, 2731–2743. [[CrossRef](#)]
13. Eringen, A.C. Nonlocal polar elastic continua. *Int. J. Eng. Sci.* **1972**, *10*, 1–16. [[CrossRef](#)]
14. Fleck, N.A.; Hutchinson, J.W. A reformulation of strain gradient plasticity. *J. Mech. Phys. Solids* **2001**, *49*, 2245–2271. [[CrossRef](#)]
15. Yang, Y.Y. Stress analysis in a joint with a functionally graded material under a thermal loading by using the Mellin transform method. *Int. J. Solids Struct.* **1998**, *35*, 1261–1287. [[CrossRef](#)]
16. Neubrand, A.; Chung, T.J.; Rödel, J.; Steffler, E.D.; Fett, T. Residual stresses in functionally graded plates. *J. Mater. Res.* **2002**, *17*, 2912–2920. [[CrossRef](#)]
17. Birman, V.; Byrd, L.W. Modeling and Analysis of Functionally Graded Materials and Structures. *Appl. Mech. Rev.* **2007**, *60*, 195. [[CrossRef](#)]
18. Şimşek, M.; Reddy, J.N. A unified higher order beam theory for buckling of a functionally graded microbeam embedded in elastic medium using modified couple stress theory. *Compos. Struct.* **2013**, *101*, 47–58. [[CrossRef](#)]
19. Reddy, J.N. Microstructure-dependent couple stress theories of functionally graded beams. *J. Mech. Phys. Solids* **2011**, *59*, 2382–2399. [[CrossRef](#)]
20. Li, L.; Hu, Y. Nonlinear bending and free vibration analyses of nonlocal strain gradient beams made of functionally graded material. *Int. J. Eng. Sci.* **2016**, *107*, 77–97. [[CrossRef](#)]
21. Javaheri, R.; Eslami, M.R. Buckling of functionally graded plates under in-plane compressive loading. *J. Appl. Math. Mech.* **2002**, *82*, 277–283. [[CrossRef](#)]
22. Ma, L.S.; Wang, T.J. Nonlinear bending and post-buckling of a functionally graded circular plate under mechanical and thermal loadings. *Int. J. Solids Struct.* **2003**, *40*, 3311–3330. [[CrossRef](#)]
23. Lanhe, W. Thermal buckling of a simply supported moderately thick rectangular FGM plate. *Compos. Struct.* **2004**, *64*, 211–218. [[CrossRef](#)]
24. Reddy, J.; Kim, J. A nonlinear modified couple stress-based third-order theory of functionally graded plates. *Compos. Struct.* **2012**, *94*, 1128–1143. [[CrossRef](#)]
25. Kim, J.; Reddy, J.N. Analytical solutions for bending, vibration, and buckling of FGM plates using a couple stress-based third-order theory. *Compos. Struct.* **2013**, *103*, 86–98. [[CrossRef](#)]
26. Ansari, R.; Faghieh Shojaei, M.; Mohammadi, V.; Gholami, R.; Darabi, M.A. Nonlinear vibrations of functionally graded Mindlin microplates based on the modified couple stress theory. *Compos. Struct.* **2014**, *114*, 124–134. [[CrossRef](#)]
27. Zhang, B.; He, Y.; Liu, D.; Shen, L.; Lei, J. An efficient size-dependent plate theory for bending, buckling and free vibration analyses of functionally graded microplates resting on elastic foundation. *Appl. Math. Model.* **2015**, *39*, 3814–3845. [[CrossRef](#)]
28. Al Jahwari, F.; Anwer, A.A.; Naguib, H.E. Fabrication and microstructural characterization of functionally graded porous acrylonitrile butadiene styrene and the effect of cellular morphology on creep behavior. *J. Polym. Sci. Part B Polym. Phys.* **2015**, *53*, 795–803. [[CrossRef](#)]

29. Al Jahwari, F.; Huang, Y.; Naguib, H.E.; Lo, J. Relation of impact strength to the microstructure of functionally graded porous structures of acrylonitrile butadiene styrene (ABS) foamed by thermally activated microspheres. *Polymer* **2016**, *98*, 270–281. [[CrossRef](#)]
30. Yadroitsev, I.; Shishkovsky, I.; Bertrand, P.; Smurov, I. Manufacturing of fine-structured 3D porous filter elements by selective laser melting. *Appl. Surf. Sci.* **2009**, *255*, 5523–5527. [[CrossRef](#)]
31. Koohbor, B.; Kidane, A. Design optimization of continuously and discretely graded foam materials for efficient energy absorption. *Mater. Des.* **2016**, *102*, 151–161. [[CrossRef](#)]
32. Giannitelli, S.M.; Basoli, F.; Mozetic, P.; Piva, P.; Bartuli, F.N.; Luciani, F.; Arcuri, C.; Trombetta, M.; Rainer, A.; Licoccia, S. Graded porous polyurethane foam: A potential scaffold for oro-maxillary bone regeneration. *Mater. Sci. Eng. C* **2015**, *51*, 329–335. [[CrossRef](#)] [[PubMed](#)]
33. Han, C.; Li, Y.; Wang, Q.; Wen, S.; Wei, Q.; Yan, C.; Hao, L.; Liu, J.; Shi, Y. Continuous functionally graded porous titanium scaffolds manufactured by selective laser melting for bone implants. *J. Mech. Behav. Biomed. Mater.* **2018**, *80*, 119–127. [[CrossRef](#)] [[PubMed](#)]
34. Chen, D.; Yang, J.; Kitipornchai, S. Free and forced vibrations of shear deformable functionally graded porous beams. *Int. J. Mech. Sci.* **2016**, *108*, 14–22. [[CrossRef](#)]
35. Shafiei, N.; Kazemi, M. Buckling analysis on the bi-dimensional functionally graded porous tapered nano-/micro-scale beams. *Aerosp. Sci. Technol.* **2017**, *66*, 1–11. [[CrossRef](#)]
36. Zhao, J.; Wang, Q.; Deng, X.; Choe, K.; Xie, F.; Shuai, C. A modified series solution for free vibration analyses of moderately thick functionally graded porous (FGP) deep curved and straight beams. *Compos. Part B Eng.* **2018**, *165*, 155–166. [[CrossRef](#)]
37. Wu, D.; Liu, A.; Huang, Y.; Huang, Y.; Pi, Y.; Gao, W. Dynamic analysis of functionally graded porous structures through finite element analysis. *Eng. Struct.* **2018**, *165*, 287–301. [[CrossRef](#)]
38. Shahverdi, H.; Barati, M.R. Vibration analysis of porous functionally graded nanoplates. *Int. J. Eng. Sci.* **2017**, *120*, 82–99. [[CrossRef](#)]
39. Wang, Y.Q.; Wan, Y.H.; Zhang, Y.F. Vibrations of longitudinally traveling functionally graded material plates with porosities. *Eur. J. Mech. A Solids* **2017**, *66*, 55–68. [[CrossRef](#)]
40. Rezaei, A.S.; Saidi, A.R.; Abrishamdari, M.; Mohammadi, M.H. Natural frequencies of functionally graded plates with porosities via a simple four variable plate theory: An analytical approach. *Thin-Walled Struct.* **2017**, *120*, 366–377. [[CrossRef](#)]
41. Thai, H.T.; Choi, D.H. A simple first-order shear deformation theory for the bending and free vibration analysis of functionally graded plates. *Compos. Struct.* **2013**, *101*, 332–340. [[CrossRef](#)]
42. Akbaş, S.D. Vibration and static analysis of functionally graded porous plates. *J. Appl. Comput. Mech.* **2017**, *3*, 199–207.
43. Wang, Y.Q.; Zu, J.W. Large-amplitude vibration of sigmoid functionally graded thin plates with porosities. *Thin-Walled Struct.* **2017**, *119*, 911–924. [[CrossRef](#)]
44. Cong, P.H.; Chien, T.M.; Khoa, N.D.; Duc, N.D. Nonlinear thermomechanical buckling and post-buckling response of porous FGM plates using Reddy's HSDT. *Aerosp. Sci. Technol.* **2018**, *77*, 419–428. [[CrossRef](#)]
45. Mirjavadi, S.S.; Afshari, B.M.; Barati, M.R.; Hamouda, A. Transient response of porous FG nanoplates subjected to various pulse loads based on nonlocal stress-strain gradient theory. *Eur. J. Mech. A Solids* **2018**, *74*, 210–220. [[CrossRef](#)]
46. Zhao, J.; Choe, K.; Xie, F.; Wang, A.; Shuai, C.; Wang, Q. Three-dimensional exact solution for vibration analysis of thick functionally graded porous (FGP) rectangular plates with arbitrary boundary conditions. *Compos. Part B Eng.* **2018**, *155*, 369–381. [[CrossRef](#)]
47. Zhao, J.; Xie, F.; Wang, A.; Shuai, C.; Tang, J.; Wang, Q. Dynamics analysis of functionally graded porous (FGP) circular, annular and sector plates with general elastic restraints. *Compos. Part B Eng.* **2019**, *159*, 20–43. [[CrossRef](#)]
48. Thang, P.T.; Nguyen-Thoi, T.; Lee, D.; Kang, J.; Lee, J. Elastic buckling and free vibration analyses of porous-cellular plates with uniform and non-uniform porosity distributions. *Aerosp. Sci. Technol.* **2018**, *79*, 278–287. [[CrossRef](#)]
49. Kim, J.; Žur, K.K.; Reddy, J.N. Bending, free vibration, and buckling of modified couples stress-based functionally graded porous micro-plates. *Compos. Struct.* **2019**, *209*, 879–888. [[CrossRef](#)]

50. Reddy, J.N. *Theory and Analysis of Elastic Plates and Shells*, 2nd ed.; CRC Press Taylor & Francis Group: Boca Raton, FL, USA, 2006.
51. Reddy, J.N. *Energy Principles and Variational Methods in Applied Mechanics*; John Wiley & Sons: Hoboken, NJ, USA, 2017.



© 2019 by the authors. Licensee MDPI, Basel, Switzerland. This article is an open access article distributed under the terms and conditions of the Creative Commons Attribution (CC BY) license (<http://creativecommons.org/licenses/by/4.0/>).